bioRxiv preprint doi: https://doi.org/10.1101/2020.07.26.221663; this version posted November 24, 2020. The copyright holder for this preprint (which was not certified by peer review) is the author/funder, who has granted bioRxiv a license to display the preprint in perpetuity. It is made available under aCC-BY-NC 4.0 International license.

Title

Laminin N-terminus α31 expression during development is lethal and causes widespread tissue-specific defects in a transgenic mouse model.

Running title: In vivo analyses of LaNt α31

Author names and affiliations

Conor J. Sugden[1], Valentina Iorio[1], Lee D. Troughton[1], Ke Liu[1], George Bou-Gharios[1]*, Kevin J. Hamill[1]*

*these authors jointly supervised this work

Affiliation: Institute of Life Course and Medical Sciences, University of Liverpool

Corresponding author (name and permanent address)

Kevin J Hamill

William Henry Duncan Building,

University of Liverpool, 6 West Derby Street,

Liverpool, UK. L7 8TX

khamill@liverpool.ac.uk

Abbreviations

LaNt α31, laminin N-terminus α31; BM, basement membrane; ECM, extracellular matrix; LN, laminin N-terminal; LM, laminin; LE, laminin-type epidermal growth factor-like domain; DMEM, Dulbecco's Modified Eagle Medium; SDS-PAGE sodium dodecyl sulfate polyacrylamide gel electrophoresis; mEFs, mouse embryonic fibroblasts; hK14, human keratin 14; intraperitoneal injection, IP

bioRxiv preprint doi: https://doi.org/10.1101/2020.07.26.221663; this version posted November 24, 2020. The copyright holder for this preprint (which was not certified by peer review) is the author/funder, who has granted bioRxiv a license to display the preprint in perpetuity. It is made available under aCC-BY-NC 4.0 International license.

Acknowledgements

We are grateful to the staff at the University of Liverpool Biomedical Services Unit. We would like to thank Dr. Takao Sakai, Dr. Rachel Lennon, and Dr. Mychel Morais for helpful discussions during the writing of this manuscript.

Conflict of interest statement

The authors declare that there are no conflicts of interests.

Author contributions:

Conor J. Sugden: Methodology, Validation, Formal analysis, Investigation, Data Curation, Writing - Original Draft, Writing - Review & Editing, Visualization. **Valentina Iorio:** Methodology, Investigation, Data Curation, Writing - Review & Editing. **Lee D. Troughton:** Methodology, Writing - Original Draft, Writing - Review & Editing. **Ke Liu:** Methodology, Writing - Review & Editing. **George Bou-Gharios:** Conceptualization, Methodology, Writing - Review & Editing, Supervision. **Kevin Hamill:** Conceptualization, Methodology, Writing - Original Draft , Writing - Review & Editing, Supervision, Funding acquisition.

Funding

This work was supported by the biotechnology and biological sciences research council [grant number BB/L020513/1] and the The University of Liverpool Crossley Barnes Bequest fund.

bioRxiv preprint doi: https://doi.org/10.1101/2020.07.26.221663; this version posted November 24, 2020. The copyright holder for this preprint (which was not certified by peer review) is the author/funder, who has granted bioRxiv a license to display the preprint in perpetuity. It is made available under aCC-BY-NC 4.0 International license.

Abstract

Laminins are essential components of all basement membranes where they regulate an extensive array of tissue functions. Alternative splicing from the laminin α3 gene produces a non-laminin but netrin-like protein, Laminin N terminus α31 (LaNt α31). LaNt α31 is widely expressed in intact tissue and is upregulated in epithelial cancers and during wound healing. In vitro functional studies have shown that LaNt α31 can influence numerous aspects of epithelial cell behaviour *via* modifying matrix organisation, suggesting a new model of laminin auto-regulation. However, the function of this protein has not been established beyond the epithelium and it has never been studied in vivo. Here, a mouse transgenic line was generated using the ubiquitin C promoter to drive inducible expression of LaNt α31. When expression was induced at embryonic day 15.5, LaNt α31 transgenic animals were not viable at birth, exhibiting localised regions of erythema. Numerous striking defects were apparent histologically, including extra-vascular erythrocytes in multiple tissues, kidney epithelial detachment, tubular dilation, interstitial bleeding, and thickening of tubule basement membranes, disruption of the epidermal basal cell layer and of the hair follicle outer root sheath, and ~50% reduction of cell numbers in the liver associated with depletion of hematopoietic erythrocytic foci. These findings demonstrate that LaNt α31 can influence tissue morphogenesis during development. More broadly, these data provide the first in vivo evidence to support an emerging model of laminin self-regulation and provide a valuable model for onward investigation into this important area.

Keywords

Laminin, netrin, basement membrane, development

bioRxiv preprint doi: https://doi.org/10.1101/2020.07.26.221663; this version posted November 24, 2020. The copyright holder for this preprint (which was not certified by peer review) is the author/funder, who has granted bioRxiv a license to display the preprint in perpetuity. It is made available under aCC-BY-NC 4.0 International license.

Summary Statement

Expression during development of Laminin N-terminus α31, a netrin-like laminin splice isoform, caused defects indicating basement membrane disruption in multiple tissues; providing the first in vivo evidence for laminin self-regulation.

bioRxiv preprint doi: https://doi.org/10.1101/2020.07.26.221663; this version posted November 24, 2020. The copyright holder for this preprint (which was not certified by peer review) is the author/funder, who has granted bioRxiv a license to display the preprint in perpetuity. It is made available under aCC-BY-NC 4.0 International license.

Introduction

Basement membranes (BMs) are specialised extracellular matrix (ECM) structures with essential and remarkably diverse roles in most cell and tissue behaviours; including regulating differentiation, cell adhesion and migration [1, 2]. BMs not only provide the mechanical attachment points that support sheets of cells to resist stresses but also influence signalling cascades via direct binding to cell surface receptors, through the sequestration and controlled release of growth factors, and by providing biomechanical cues, as reviewed in [3, 4]. BMs are also dynamic structures that are remodelled in terms of composition and structure throughout life, with the most striking changes occuring during development [5, 6]. At the core of every BM are two networks of structural proteins; type IV collagens and laminins (LMs)[7].

Each LM is an obligate αβγ heterotrimer formed from one of five α chains (*LAMA1-5*), three β chains (*LAMB1-3*) and three γ chains (*LAMC1-3*), with each chain displaying spatio-temporal distribution patterns, as reviewed in [8-11]. Assembly of LM networks and higher-order structures involves formation of a ternary node between the laminin N-terminal (LN) domains of an α, a β and a γ chain [12, 13]. These ternary αβγ nodes assemble in a two-step process involving an initial rapid formation of unstable βγ LN intermediate which is then stabilised through the incorporation of an α LN domain [14-17]. The biological importance of these LN-LN interactions is exemplified by a group of human syndromic disorders where missense mutations affecting the LN domains of the *LAMA2*, *LAMB2* or *LAMA5* genes give rise to muscular dystrophy in merosin-deficient muscular dystrophy, kidney and ocular developmental defects in Pierson syndrome, or defects in kidney, craniofacial and limb development respectively [18-22]. Although these disorders demonstrate that LM network assembly is essential for homeostasis of numerous tissues, not all LM chains contain an LN domain. Specifically, LMα4, which is expressed at high levels in the vasculature, and the LMα3a and LMγ2 chains, which are abundant in surface epithelium including the skin, have shortened amino termini which lack this key domain but yet still form functional BMs [8, 9, 23, 24]. This raises questions of whether LN domains are important in all tissue contexts or whether additional proteins may compensate for the inability of the LMs to form networks.

bioRxiv preprint doi: https://doi.org/10.1101/2020.07.26.221663; this version posted November 24, 2020. The copyright holder for this preprint (which was not certified by peer review) is the author/funder, who has granted bioRxiv a license to display the preprint in perpetuity. It is made available under aCC-BY-NC 4.0 International license.

Alongside their main LM transcripts, the *LAMA3* and *LAMA5* genes produce short transcripts encoding proteins that are unable to trimerise into LMs but which contain LN domains [25]. At least one of these laminin N terminus proteins encodes a functional protein, LaNt α31, the structural features of which are an α LN domain followed by a short stretch of laminin-type epidermal growth factor-like (LE) domains and unique C-terminal region with no conserved domain architecture. In addition to the LaNt proteins, the laminin-superfamily includes netrin genes which encode proteins with either β or γ LN domains, stretches of LE repeats and unique C-terminal regions (as reviewed in [26]. Moreover, proteolytic processing of LMs are also released from LMα1 [27], LMβ1 [28], LMα3b [29]. Each of these LN domain-containing proteins and cryptic fragments have cell surface receptor binding capabilities and can act as signalling molecules (reviewed in [30]. However, netrin-4, which evolved independently from the other netrins [31, 32], also has LM-network disrupting capabilities [33, 34], and when overexpressed in vivo, caused increased lymphatic permeability [35]. Netrin-4 LN domain has greatest homology with LM β LN domains whereas LaNt α31 contains the LMα3b LN domain [36]; therefore, although LaNt α31 could act similarly to these proteins, it likely plays a different role depending on the LM context.

LaNt α31 is expressed in the basal layer of epithelia in the skin [25], cornea [37] and digestive tract, the ECM around terminal duct lobular units of the breast and alveolar air sacs in the lung, and is widely expressed by endothelial cells [38]. Increased expression is associated with breast ductal carcinoma and in vitro overexpression leads to a change in the mode of breast cancer cell invasion through LM-rich matrices [39]. LaNt α31 is also transiently upregulated during re-epithelialization ex vivo burn wounds and in stem cell activation assays [37]. In epidermal and corneal keratinocytes, knockdown or overexpression experiments revealed that modulating LaNt α31 levels leads to reduced migration rates and modifying cell-to-matrix adhesion [25, 40]. Consistent with a role in matrix assembly, increased expression LaNt α31 causes striking changes to LM332, including formation tight clusters beneath cells and increasing the proteolytic processing of LMα3 by matrix metalloproteinases [40]. Although these findings all support LaNt α31 as being a mediator of cell behaviour, it is as yet unknown what role it plays in complex in vivo tissue environments and in particualar in matrixes that are actively being remodeled.

bioRxiv preprint doi: https://doi.org/10.1101/2020.07.26.221663; this version posted November 24, 2020. The copyright holder for this preprint (which was not certified by peer review) is the author/funder, who has granted bioRxiv a license to display the preprint in perpetuity. It is made available under aCC-BY-NC 4.0 International license.

Here, we present the first in vivo study of LaNt α31 overexpression in newly developed mouse models.

bioRxiv preprint doi: https://doi.org/10.1101/2020.07.26.221663; this version posted November 24, 2020. The copyright holder for this preprint (which was not certified by peer review) is the author/funder, who has granted bioRxiv a license to display the preprint in perpetuity. It is made available under aCC-BY-NC 4.0 International license.

Materials and methods

Ethics

All procedures were licensed by the UK Home Office under the Animal (Specific Procedures) Act 1986, project license numbers (PPL) 70/9047 and 70/7288. All mice were housed and maintained within the University of Liverpool Biological Services Unit in specific pathogen-free conditions in accordance with UK Home Office guidelines. Food and water were available ad libitum.

Antibodies

Rabbit monoclonal antibodies against the influenza hemagglutinin epitope (HA) (C29F4, Cell Signalling Technology, Danvers, MA) were used for immunoblotting at 67 ng ml^{-1}. Goat polyclonal antibodies against DDDDK (equivalent to FLAG sequence, ab1257, Abcam, Cambridge, UK), rabbit polyclonal antibodies against 6X-His (ab137839, Abcam), and rabbit polyclonal antibodies against lamin A/C (4C11, Cell Signalling Technology) were used at 1 µg ml^{-1} for immunoblotting. Mouse monoclonal antibodies against LaNt α31 [37] were used at 0.225 µg ml^{-1} for immunoblotting. Rabbit polyclonal antibodies against mCherry (ab183628, Abcam) were used at 2.5 µg ml^{-1} for immunofluorescence. Alexa fluor 647 conjugated goat anti-rabbit IgG recombinant secondary antibodies, were obtained from Thermo Fisher Scientific (Waltham, MA, United States) and used at 2 µg ml^{-1} for indirect immunofluorescence microscopy.

pUbC-LoxP-LaNtα31-T2A-tdTomato

A gBlock was synthesised (Integrated DNA Technologies, Coralville, IA) containing *Nde*I and *Nde*I restriction enzyme sites, T7 promoter binding site [41], Kozak consensus sequence [42], Igκ secretion signal (METDTLLLWVLLLWVPGSTGD) [43], LaNt α31-encoding cDNA (amino acids 38-488) [25], Flag (DYKDDDDK) [44] and HA (YPYDVPDYA) [45] tag sequences, T2A sequence (EGRGSLLTCGDVEENPGP) [46], and *BamH*I. The gBlock DNA was inserted into pCSCMV:tdTomato (a gift from Gerhart Ryffel, Addgene plasmid #30530 ; http://n2t.net/addgene:30530; RRID:Addgene_30530) using *Nde*I and *BamH*I (New England Biolabs, Ipswich, MA), to produce pCS-LaNtα31-T2A-tdTomato. LaNtα31-T2A-tdTomato

bioRxiv preprint doi: https://doi.org/10.1101/2020.07.26.221663; this version posted November 24, 2020. The copyright holder for this preprint (which was not certified by peer review) is the author/funder, who has granted bioRxiv a license to display the preprint in perpetuity. It is made available under aCC-BY-NC 4.0 International license.

was then removed from this backbone using *Nhe*I and *EcoR*I, and inserted into a vector containing the Ubiquitin C (UbC) promoter and a floxed stop cassette, all flanked by cHS4 insulator elements, producing pUbC-LoxP-LaNtα31-T2A-tdTomato.

hK14-LaNt α31

Full length LaNt α31 cDNA was amplified by PCR and inserted into pSecTag vector (Thermo Fisher Scientific), introducing Igκ leader sequence 5' of the LaNt α31 sequence, and Myc and 6x His tags 3' of the LaNt α31 sequence. The complete Igκ-LaNt α31-Myc-His sequence was inserted into pGEM®-5Zf(+) vector (Promega, Madison, WI) using *Nhe*I and *Pme*I (New England Biolabs), producing pGEM®-5Zf(+)-LaNt α31. Separately, the sequence encoding human keratin 14 (hk14) promoter was amplified by PCR, using primers introducing *Mlu*I 5' and *Nde*I, *Nsi*I 3' of the sequence, and this was inserted into a bicistronic vector containing the mCherry seqeunce, producing phK14-mCherry. Finally, Igκ-LaNtα31-Myc-His was excised from pGEM®-5Zf(+)-LaNtα31 using *Nde*I and *Nsi*I (New England Biolabs) and inserted into phK14-mCherry, to produce phK14-LaNtα31-T2A-mCherry.

Cloning procedures

Restriction digests were set up with 1 µg of plasmid DNA, 1 µg of PCR product, or 100 ng of gBlock DNA, 20 U of each enzyme and CutSmart buffer (50 mM Potassium Acetate, 20 mM Tris-acetate, 10 mM magnesium acetate, 100 µg ml^{-1} BSA (New England Biolabs) and incubated at 37°C for 1 h. Enzymatic activity was inactivated by 20 min incubation at 65°C. PCR or cloning products were separated using 1% (w/v) agarose gels (Thermo Fisher Scientific) dissolved in 1 x TAE electrophoresis buffer (40 mM Tris pH 7.6, 20 mM acetic acid, 1 mM EDTA) containing ethidium bromide, and visualised using a UV transilluminator ChemiDoc MP System (BioRad, Hercules, CA). DNA bands of the correct sizes were excised from the gel and purified using GenElute™ Gel Extraction Kit, following manufacturer's protocol (Sigma Aldrich, St. Louis, Missouri, United States). Purified inserts were ligated into vectors at 3:1 molar ratios, either using Instant Sticky-end Ligase Master Mix (New England Biolabs) following manufacturers protocol, or using 400 U of T4 DNA ligase and 1X reaction buffer (50 mM Tris-HCl, 10 mM $MgCl_2$ 1 mM

bioRxiv preprint doi: https://doi.org/10.1101/2020.07.26.221663; this version posted November 24, 2020. The copyright holder for this preprint (which was not certified by peer review) is the author/funder, who has granted bioRxiv a license to display the preprint in perpetuity. It is made available under aCC-BY-NC 4.0 International license.

ATP, 10 mM DTT, New England Biolabs) at 16°C overnight, followed by enzymatic inactivation at 65°C for 10 min. Ligated DNA was heat-shock transformed into One-Shot TOP10 chemically competent E. coli cells (Thermo Fisher Scientific) following manufacturer's protocol, then plated onto LB plates containing the appropriate antibiotic (100 µg ml^{-1} ampicillin, 50 µg ml^{-1} kanamycin or 25 µg ml^{-1} chloramphenicol, Sigma Aldrich). Plasmid DNA was extracted from bacteria using GenElute™ Plasmid Miniprep Kit (Sigma Aldrich), following the manufacturer's protocol. Plasmids were sequenced by DNASeq (University of Dundee, Dundee, UK).

Cell Culture

KERA-308 murine epidermal keratinocyte cells [47], were purchased from CLS (Cell Lines Service GmbH, Eppelheim, Germany) and maintained in high glucose (4.5 g L^{-1}) Dulbecco's Modified Eagle Medium (DMEM, Sigma Aldrich) supplemented with 10% foetal calf serum (LabTech, East Sussex, UK) and 2 mM L-glutamine (Sigma Aldrich). HEK293A cells were maintained in DMEM supplemented with 10% FCS and 4 mM L-glutamine.

Cell Transfections

1 x 10□ KERA-308 or 4 x 10^5 HEK293A cells were seeded in 6-well plates (Greiner-BioOne, Kremsmünster, Austria) 24 h prior to transfection. For KERA-308 cells, 2 µg of hK14-LaNtα31-T2A-mCherry or LaNt-α31-pSec-Tag and 2 µl Lipofectamine 2000 (Thermo Fisher Scientific) were used. For HEK293A cells, either 1 µg pCAG-Cre:GFP and 2 µl Lipofectamine 2000, 2 µg of pUbC-LoxP-LaNtα31-T2A-tdTomato and 5 µl Lipofectamine 2000, or 2 µg of pUbC-LoxP-LaNtα31-T2A-tdTomato, 1 µg of pCAG-Cre:GFP and 7 µl Lipofectamine 2000 (Thermo Fisher Scientific), were mixed with 2 ml of Gibco™ Opti-MEM™ Reduced Serum Medium (Thermo Fisher Scientific) and incubated for 10 min at room temperature. The DNA-lipofectamine complex was added to the wells, and the media was replaced with DMEM high glucose after 6 h.

bioRxiv preprint doi: https://doi.org/10.1101/2020.07.26.221663; this version posted November 24, 2020. The copyright holder for this preprint (which was not certified by peer review) is the author/funder, who has granted bioRxiv a license to display the preprint in perpetuity. It is made available under aCC-BY-NC 4.0 International license.

Explant culture method

Hair was removed from mouse skin tissue using Veet hair removal cream (Reckitt Benckiser, Slough, UK) and the skin washed in Dulbecco's Phosphate Buffered Saline (DPBS) containing 200 U ml^{-1} penicillin, 200 U ml^{-1} streptomycin, and 5 U ml^{-1} amphotericin B1 (all Sigma Aldrich). The skin was then dissected into 2-3 mm^2 pieces using a surgical scalpel and 3 or 4 pieces placed per well of a 6-well dish (Greiner Bio-One, Kremsmünster, Austria) with the dermis in contact with the dish. 300 µl of DMEM supplemented with 20% FCS, 2 mM L-glutamine, 200 µg ml^{-1} penicillin, 200 µg ml^{-1} streptomycin, and 5 µg ml^{-1} fungizone (all Sigma Aldrich) was added to the wells. After 24 h, each well was topped up with 1 ml of media, and the media was replenished every 48 h thereafter.

Transgenic Line establishment

Generation of transgenic mice were carried out based on the protocol described in [48]. C57Bl6CBAF1 females (Charles River Laboratories, Margate, Kent, UK) between 6-8 weeks were superovulated by intraperitoneal (IP) injections of 5 IU pregnant mare's serum gonadotrophin (PMSG; in 100µl H_2O), followed 46 h later by 5 IU of human chorionic gonadotropin (hCG, Sigma Aldrich). Treated females were mated with C57Bl6CBAF1 males overnight. Mated females were identified from the presence of copulation plugs, anaesthetised, and oviducts removed and dissected in M2 media (Millipore, Watford, UK). Day-1 oocytes (C57BL/6Jx CBA F1) were transferred into clean media by mouth pipetting. Cumulus cells were removed by hyaluronidase (300 µg ml^{-1}, Merck, Darmstadt, Germany) treatment in M2 media with gentle shaking until detached from the egg surface. Oocytes were then rinsed and transferred to M16 media (Millipore, Speciality Media, EmbryoMax) ready for injection.

DNA was diluted to a final concentration of 2 ng μl^{-1} in embryo water (Sigma Aldrich) and filter-purified using Durapore-PVDF 0.22 µM centrifuge filters (Merck). Injection pipettes were used to pierce the outer layers of the oocyte and to inject DNA. DNA was injected into the pronuclei of the oocyte. Undamaged eggs were transferred to clean M16 media and incubated at 37°C until transferred into pseudopregnant CD1 females on the same day. Meanwhile, pseudopregnant females were obtained by mating vasectomised CD1 males overnight. Copulation plugs were checked and females were used 1 day

bioRxiv preprint doi: https://doi.org/10.1101/2020.07.26.221663; this version posted November 24, 2020. The copyright holder for this preprint (which was not certified by peer review) is the author/funder, who has granted bioRxiv a license to display the preprint in perpetuity. It is made available under aCC-BY-NC 4.0 International license.

post-coitum. Females were anaesthetised by inhalation of isoflurane (Sigma Aldrich). 30 injected oocytes were transferred to plugged pseudopregnant female oviducts through the infundibulum.

In generating the pUbC-LoxP-LaNtα31-T2A-tdTomato line, 460 mouse zygotes were injected over four sessions. 87% of these zygotes survived and were transferred into 11 recipient CD1 mothers. From these mothers, 42 pups were born. Of the 10 F0 mice that gave a positive genotype result, four passed on the transgene to the F1 generation. Mice that did not pass on the transgene to the F1 generation were culled, the four F0 mice were mated to expand colonies for cryopreservation, and one line was continued for investigation.

For K14-LaNtα31 transgenic mice, 140 embryos were transferred into five recipient CD1 mothers. Three small litters were born, totalling seven pups. two pups possessed the transgene, and these were mated to generate F1 mice.

R26CreERT2 (Jax Lab 008463) [49] mice were purchased from The Jackson Laboratory (Bar Harbor, Maine, United States).

In Vivo Transgene Induction

Tamoxifen (Sigma Aldrich) was dissolved in corn oil (Sigma Aldrich) and administered via IP at a concentrations of 25 mg kg^{-1} or 75 mg kg^{-1}. Progesterone (Sigma Aldrich) was dissolved in corn oil (Sigma Aldrich) and was co-administered alongside tamoxifen at a dose of exactly half of the corresponding tamoxifen dose (12.5 mg kg^{-1} or 25 mg kg^{-1}).

DNA Extraction

Four weeks after birth, ear notches were collected from mouse pups and digested in 100 µl lysis buffer (50 mM Tris-HCl pH 8.0, 0.1 M NaCl, 1% SDS, 20 mM EDTA) and 10 µl of proteinase K (10 mg ml^{-1}, all Sigma Aldrich) overnight at 55°C. The following day, samples were cooled, spun at 13,000 rpm for 3 min and the supernatant transferred to clean 1.5 ml tubes (Eppendorf, Hamburg, Germany). An equal volume of isopropanol (Sigma Aldrich) was added, gently inverted and span at 13,000 rpm, and supernatant

bioRxiv preprint doi: https://doi.org/10.1101/2020.07.26.221663; this version posted November 24, 2020. The copyright holder for this preprint (which was not certified by peer review) is the author/funder, who has granted bioRxiv a license to display the preprint in perpetuity. It is made available under aCC-BY-NC 4.0 International license.

discarded. Pellets were washed with 500 µl of 70% EtOH (Sigma Aldrich), then air-dried for 10 min, and resuspended in 50 µl ddH_20.

PCR

50 ng of genomic DNA was mixed with 12.5 µl of REDtaq ReadyMix PCR Reaction Mix (20 mM Tris-HCl pH 8.3, 100 mM KCl, 3 mM MgCl2, 0.002% gelatin, 0.4 mM dNTP mix, 0.06 unit/ml of Taq DNA Polymerase, Sigma Aldrich) and 0.5 µM of each primer; ddH_20 was added to make the reaction mixture up to 25 µl. Primer pairs for genotyping were as follows: LaNt α31 to tdTomato Forward 5' – ATCTATGCTGGTGGAGGGGT – 3', Reverse 5' – TCTTTGATGACCTCCTCGCC – 3'; Cre Forward 5' – GCATTACCGGTCGATGCAACGAGTGATGAG – 3', Reverse 5' – GAGTGAACGAACCTGGTCGAAATCAGTGCG – 3'; Recombination Forward 5' – TCCGCTAAATTCTGGCCGTT – 3', Reverse 5' – GTGCTTTCCTGGGGTCTTCA – 3'(all from Integrated DNA Technologies). Cycle conditions were as follows: Genotyping – 1 cycle of 95°C for 5 min, 35 cycles of 95°C for 15 s; 56°C for 30 s; 72°C for 40 s, followed by a final cycle of 72°C for 5 min. For checking recombination: 1 cycle of 95°C for 5 min, 35 cycles of 95°C for 15 s; 60°C for 30 s; 72°C for 90 s, followed by a final cycle of 72°C for 7 min. PCR products were separated by gel electrophoresis and imaged using a BioRad Gel Doc XR+ System.

SDS-PAGE and western immunoblotting

Cells were homogenized by scraping into 90 µL Urea/SDS buffer: 10 mM Tris-HCl pH 6.8, 6.7 M urea, 1% w/v SDS, 10% v/v glycerol and 7.4 µM bromophenol blue, containing 50 µM phenylmethysulfonyl fluoride (PMSF) and 50 µM N-methylmaleimide (all Sigma Aldrich). Lysates were sonicated and 10% v/v β-mercaptoethanol (Sigma Aldrich) added. Proteins were separated by sodium dodecyl sulfate-polyacrylamide gel electrophoresis (SDS-PAGE) using 10% polyacrylamide gels; 1.5 M Tris, 0.4% w/v SDS, 10% acrylamide/ bis-acrylamide (all Sigma Aldrich), electrophoresis buffer; 25 mM tris-HCl, 190 mM glycine, 0.1% w/v SDS, pH 8.5 (all Sigma Aldrich). Proteins were transferred to a nitrocellulose membrane using the TurboBlot™ system (BioRad) and blocked at room temperature in

bioRxiv preprint doi: https://doi.org/10.1101/2020.07.26.221663; this version posted November 24, 2020. The copyright holder for this preprint (which was not certified by peer review) is the author/funder, who has granted bioRxiv a license to display the preprint in perpetuity. It is made available under aCC-BY-NC 4.0 International license.

Odyssey® TBS-Blocking Buffer (Li-Cor BioSciences, Lincoln, NE, United States) for 1 h. The membranes were probed overnight at 4°C diluted in blocking buffer, washed 3 x 5 min in PBS with 0.1% Tween (both Sigma Aldrich) and probed for 1 h at room temperature in the dark with IRDye® conjugated secondary Abs against goat IgG (800CW) and rabbit IgG (680CW), raised in goat or donkey (LiCor BioSciences), diluted in Odyssey® TBS-Blocking Buffer at 0.05 µg ml^{-1}. Membranes were then washed for 3 x 5 min in PBS with 0.1% Tween, rinsed with ddH_2O and imaged using the Odyssey® CLX 9120 infrared imaging system (LiCor BioSciences). Image Studio Light v.5.2 was used to process scanned membranes.

Tissue processing

For cryosections, P0 pups were culled by cervical dislocation, and fixed in 4% paraformaldehyde (Merck) overnight at 4°C. Samples were cryoprotected in 30% sucrose/PBS solutions then in 30% sucrose/PBS:O.C.T (1:1) solutions (Tissue-Tek, Sakura Finetek Europe, Alphen aan den Rijn, The Netherlands), each overnight at 4°C. Samples were embedded in OCT compound and transferred on dry ice. Embedded samples were sectioned at 8 µm using a Leica CM1850 cryostat (Leica, Wokingham, UK). For paraffin sections, Tissues were fixed in 10% neutral buffered formalin (Leica,) for 24 h, then processed through graded ethanol and xylene before being embedded in paraffin wax. 5 µm sections were cut using a rotary microtome RM2235 (Leica), adhered to microscope slides, then dried overnight at 37°C. Sections were dewaxed and rehydrated with xylene followed by a series of decreasing ethanol concentrations. Antigen retrieval was performed by microwaving sections in preheated 0.01 M citrate buffer pH 6 (Sigma Aldrich) for 5 min.

Hematoxylin and Eosin Staining

Sections were dewaxed and rehydrated with xylene followed by a series of decreasing ethanol concentrations. Sections were then stained in Harris hematoxylin solution (Leica) for 5 min, H_2O for 1 min, acid alcohol (Leica) for 5 s, H_2O for 5 min, aqueous eosin (Leica) for 3 min, H_2O for 15 s, followed by dehydration through graded ethanol and xylene. Slides were coverslipped with DPX mounting media (Sigma Aldrich).

bioRxiv preprint doi: https://doi.org/10.1101/2020.07.26.221663; this version posted November 24, 2020. The copyright holder for this preprint (which was not certified by peer review) is the author/funder, who has granted bioRxiv a license to display the preprint in perpetuity. It is made available under aCC-BY-NC 4.0 International license.

Immunohistochemistry

Slides were incubated in ice-cold acetone for 10 min, then transferred into PBS for 10 minblocking, then blocked in PBS containing 10% normal goat serum (NGS) at room temperature for 1 h. Next, samples were probed with the primary antibodies diluted in PBS-Tween (0.05%) with 5% NGS at 4°C overnight. Samples were then washed for 3 x 5 min in PBS-Tween (0.05%), before being probed with secondary antibodies diluted in PBS-Tween (0.05%) with 5% NGS at room temperature for 1 h. Samples were washed for 3 x 5 min in PBS-Tween (0.05%). Slides were mounted with VECTASHIELD® Antifade Mounting Medium with DAPI (VECTASHIELD®, Burlingame, CA).

Image Acquisition

H&E images were acquired using a Zeiss Axio Scan.Z1 equipped with an Axiocam colour CCD camera using ZEN Blue software (all from Zeiss, Oberkochen, Germany). Live cell images were acquired using a Nikon Eclipse Ti-E microscope (Nikon, Tokyo, Japan). Immunofluorescence images of tissues were acquired using a Zeiss LSM 800 confocal microscope (Zeiss).

Image Analysis

Images were processed using either Zen 2.6 (blue edition) (Zeiss) or ImageJ (National Institutes of Health, Bethesda, MD, United States)[50]. Stardist plugin [51] was used for segmentation of nuclei from H&E images. Images were thresholded manually to remove areas containing no tissue in the images.

bioRxiv preprint doi: https://doi.org/10.1101/2020.07.26.221663; this version posted November 24, 2020. The copyright holder for this preprint (which was not certified by peer review) is the author/funder, who has granted bioRxiv a license to display the preprint in perpetuity. It is made available under aCC-BY-NC 4.0 International license.

Results

Inducible LaNt α31 construct validation.

To investigate the consequences of LaNt α31 overexpression in vivo, we generated an inducible system for conditional LaNt α31 transgene expression (Fig. 1A). An expression construct was created containing the ubiquitin C promoter driving expression of the human LaNt α31 cDNA with the native secretion signal replaced by mouse immunoglobulin κ leader sequence to maximise secretion, and with sequences for Flag and HA epitope tags added to the C-terminus of the LaNt α31 coding region. A T2A element was included to enable expression of tdTomato from the same transgene but not directly fused to LaNt α31 [46]. A floxed stop-cassette was inserted between the promoter and the start of the construct to prevent transgene expression until Cre-mediated removal of this cassette. The entire construct was flanked with the cHS4 β-globin insulator to protect against chromatin-mediated gene silencing [52] (Fig. 1A). Restriction enzyme digests and plasmid sequencing confirmed the assembled pUbC-LoxP-LaNtα31-T2A-tdTomato plasmid.

To confirm the construct expressed only following exposure to Cre recombinase, the pUbC-LoxP-LaNtα31-T2A-tdTomato was co-transfected alongside pCAG-Cre:GFP, encoding GFP-tagged Cre recombinase, into HEK293A cells. tdTomato signal was observed only in cells transfected with both plasmids (Fig. 1B). PCR using primers flanking the STOP cassette also confirmed that the cassette was removed only in cells transfected with both plasmids (Fig. 1C). Western blotting using polyclonal anti-Flag antibodies confirmed expression of the predicted ~ 57 kDa band in co-transfected cell lysates (Fig. 1D), this also confirmed that the T2A element was cleaved in the final product releasing the tdTomato tag. Together, these results demonstrate that the pUbC-LoxP-LaNtα31-T2A-tdTomato plasmid allows for the Cre-inducible expression of LaNt α31 and tdTomato.

Generation and validation of a novel LaNt α31 overexpressing mouse line.

The pUbC-LoxP-LaNtα31-T2A-tdTomato construct was linearised, and transgenic F0 mice generated by pronuclear microinjection into oocytes. To confirm transgene expression, F0 mice were mated with WT (C57BL/6J) mice, embryos were collected at E11.5, and mEFs were isolated from the embryos.

bioRxiv preprint doi: https://doi.org/10.1101/2020.07.26.221663; this version posted November 24, 2020. The copyright holder for this preprint (which was not certified by peer review) is the author/funder, who has granted bioRxiv a license to display the preprint in perpetuity. It is made available under aCC-BY-NC 4.0 International license.

Presence of the UbC-LoxP-LaNtα31-T2A-tdTomato transgene (hereafter UbCLaNt) was confirmed by PCR (Fig. 2A). mEFs were transduced with an adenovirus encoding codon-optimised Cre recombinase (ad-CMV-iCre). Analysis by immunoblotting with anti-HA-antibodies (Fig. 2B) revealed a ~57 KDa band and fluorescence microscopy confirmed tdTomato expression (Fig. 2C) in samples containing both the UbC-LaNt transgene and the ad-CMV-iCre, but not in cells with either plasmid individually.

Male UbCLaNt mice were mated with females from the tamoxifen-inducible ubiquitous Cre line R26CreERT2 (Fig. 3A). Transgene expression was induced by IP of tamoxifen at E13.5, and embryos collected at E19.5. PCR confirmed that Cre/LoxP mediated recombination only occurred in the embryos with both the UbCLaNt and the R26CreERT2 (Fig. 3B). Explants were generated from the skin of these embryos, and only the explants grown from double transgenic embryos exhibited tdTomato expression by fluorescence microscopy (Fig. 3C) and HA-tagged LaNt α31 expression by western immunoblotting (Fig. 3D). Together, these data confirmed the generation of tamoxifen-inducible LaNt α31 overexpressing mouse line, without detectable leakiness (UbCLaNt::R26CreERT2).

UbCLaNt::R26CreERT2 expression in utero causes death and localised regions of erythema at birth.

To determine the impact of LaNt α31 during development where extensive BM remodelling occurs, tamoxifen was administered via IP to pregnant UbCLaNt::R26CreERT2 mice at E15.5 and pregnancies allowed to continue to term. Across two litters from different mothers, two from six pups and three from five pups respectively were intact but not viable at birth, while the remaining littermates were healthy. The non-viable pups displayed localised regions of erythema with varying severity between the mice, but were otherwise fully developed and the same size as littermates (Fig. 4A). Genotyping identified that all offspring possessed both the UbCLaNt and R26CreERT2 transgenes (Fig. 4B). Hereafter, non-viable pups are referred to as UbCLaNt::R26CreERT2 1E1, 1E2, 2E1, 2E2, 2E3, and viable pups UbCLaNt::R26CreERT2 2NE1, 2NE2. To confirm transgene expression, skin explants were established from non-viable pups, and tdTomato fluorescence was confirmed by microscopy (Fig. 4C). Consistent with the fluorescence data, western immunoblot analysis of total protein extracts from the explanted cells and whole embryo lysates revealed transgene expression in non-viable pups, although expression levels varied between the mice (Fig. 4D). To

bioRxiv preprint doi: https://doi.org/10.1101/2020.07.26.221663; this version posted November 24, 2020. The copyright holder for this preprint (which was not certified by peer review) is the author/funder, who has granted bioRxiv a license to display the preprint in perpetuity. It is made available under aCC-BY-NC 4.0 International license.

further confirm transgene expression within tissues, OCT-embedded skin sections of UbCLaNt::R26CreERT2 were processed with anti-mCherry antibodies which recognise the tdTomato protein, revealing that only the non-viable pups expressed the tdTomato reporter (Fig. 4E). Together these data confirm that only non-viable mice expressed the LaNt α31 transgene

To identify LaNt α31 effects at the tissue level, the pups were formalin-fixed and paraffin-embedded then processed for H&E and immunohistochemistry. All organs were present in the mice and appeared intact at the macroscopic level; however, blood exudate was observed throughout multiple tissues in all of the LaNt α31 transgene expressing mice. We focused our attention on kidney, skin and lung as examples of tissues where the BMs with differences in LM composition and where we hypothesised LaNt α31 could, therefore, elicit distinct effects. Specifically, the predominant LMs in the kidney contain three LN domains, and mutations affecting LM polymerisation lead to Pierson syndrome [19, 53-56], whereas the major LM in the skin contains one LN domain, LM332, and loss of function leads to skin fragility, reviewed in [57], and granulation tissue disorders [58, 59]. In the lung, LM311, a two LN domain LM, is enriched [60, 61] and absence of LMα3 is associated with pulmonary fibrosis [62]. Each of these three tissues also express LaNt α31 in adult human tissue, and are, therefore, tissues where dysregulation of expression regulation could be physiologically relevant [38].

LaNt α31 overexpression leads to epithelial detachment, tubular dilation and interstitial bleeding in the kidney.

In the kidneys, striking alterations were observed in the renal tubules, pelvis, and blood vessels of UbCLaNt::R26CreERT2 mice expressing the transgene. Specifically, dilation and detachment of the lining epithelia in collecting ducts and uteric bud segments was evident (Fig. 5A, black arrows), and changes were observed in the vessels of the kidney, with bleeding into the interstitial and subtubular surroundings (Fig. 5A, yellow arrows). There was some severity in the extent of the defects between the expressing pups (interstitial bleeding 4 out of 5 mice, pelvic dilation 2 out of 5, epithelial detachment and tubular observed in all mice). Indirect IF processing of tissue using antibodies raised against LM111 revealed LM localisation to

bioRxiv preprint doi: https://doi.org/10.1101/2020.07.26.221663; this version posted November 24, 2020. The copyright holder for this preprint (which was not certified by peer review) is the author/funder, who has granted bioRxiv a license to display the preprint in perpetuity. It is made available under aCC-BY-NC 4.0 International license.

be unchanged, however immunoreactivity of the tubule BMs was thickened in the expressing pups compared with littermate controls (Fig. 5B).

LaNt α31 overexpression disrupts epithelial basal cell layer organisation.

Histological examination of the dorsal skin of UbCLaNt::R26CreERT2 mice revealed localised disruption of the epidermal basal cell layer, with a loss of the tight cuboidal structure of the stratum basale (Fig. 6A). Basal layer disruption was also observed in the outer root sheath of the hair follicles (Fig. 6A). Although no evidence of blistering at the dermal-epidermal junction was observed Mice expressing the LaNt α31 transgene displayed discontinuous LM immunoreactivity at the epidermal-dermal junction (Fig. 6B). However, the LM surrounding the outer root sheath was unaffected (Fig. 6B).

Mice expressing the LaNt α31 transgene display structural differences in the lung.

Lungs of P0 mice were not inflated prior to FFPE, however structural differences between non-expressing and expressing mice were apparent. Specifically, in mice expressing LaNt α31, fewer, less densely packed alveolar epithelial cells were observed. Additionally, and similarly to the kidney, erythrocytes were present throughout the lung tissue. (Fig. 7A).

LaNt α31 overexpression leads to a reduction of hematopoietic colonies in the liver.

Surprisingly, drastic and obvious superficial changes were apparent in the livers of mice expressing the LaNt α31 transgene compared to the non-expressing mice. Although the bile ducts, sinusoid endothelium and hepatocyte morphology were unchanged, there was a clear reduction in hematopoietic foci in the LaNt α31 transgene expressing animals (Fig. 7B). This reduction corresponded to a >48% reduction of total cell number (WT= 11.5 nuclei/ mm^2, mean NE = 11.4 nuclei/ mm^2, mean E= 5.8 nuclei/ mm^2; Fig. 7C, D).

bioRxiv preprint doi: https://doi.org/10.1101/2020.07.26.221663; this version posted November 24, 2020. The copyright holder for this preprint (which was not certified by peer review) is the author/funder, who has granted bioRxiv a license to display the preprint in perpetuity. It is made available under aCC-BY-NC 4.0 International license.

Keratin 14-driven constitutive LaNt α31 induces a low offspring number.

We next used a keratin-14 promoter (K14) to restrict expression to skin and the epithelia of tongue, mouth, forestomach, trachea, thymus and respiratory and urinary tracts [63-65]. K14 promoter activity has also been described in the oocyte [66]. The new construct used the human K14 promoter drive expression of human LaNt α31, followed by a T2A element and a mCherry reporter Fig. S1A) and was validated by transfecting into KERA 308 mouse epidermal keratinocytes and visualising the mCherry fluorescence (Fig. S1B) and immunoblotting for the LaNt α31 protein (Fig. S1C).

K14-LaNtα31 transgenic mice were generated by pronuclear microinjection. However, unusually small litters were obtained from recipient CD1 mothers and mice containing the transgene DNA (Fig. S1D) did not express the transgene at the protein level (Fig. S1F-G). The unusually low offspring sizes, combined with the lack of protein expression in genotype-positive mice, suggests that expression of LaNt α31 under the control of the K14 promoter is lethal during development.

bioRxiv preprint doi: https://doi.org/10.1101/2020.07.26.221663; this version posted November 24, 2020. The copyright holder for this preprint (which was not certified by peer review) is the author/funder, who has granted bioRxiv a license to display the preprint in perpetuity. It is made available under aCC-BY-NC 4.0 International license.

Discussion

This study has demonstrated that LaNt α31 overexpression ubiquitously during development is lethal, causing tissue specific-defects. These defects include blood exudate throughout most tissues as well as striking changes to the tubules of the kidney and the basal layer of the epidermis, depletion of hematopoietic colonies in the liver, and evidence of BM disruption at the dermal-epidermal junction. These findings build upon previous in vitro and ex vivo work that have implicated LaNt α31 in the regulation of cell adhesion, migration, and LM deposition[25, 37, 40]. These findings provide the first in vivo evidence that this little-studied *LAMA3*-derived splice isoform has biological significance in BM and tissue formation during development and provide a valuable platform for onward investigation.

The molecular mechanism behind the severe phenotype of the transgenic animals is challenging to determine at this point, however we can provide several plausible reasons that can explain the phenotype with substantial overlap. As LM network assembly requires binding of an α, β and γ LN domain [14-17, 67], we predicted that the presence of an α LN domain within LaNt α31 would influence LM-LM interactions and therefore BM assembly or integrity. Consistent with this hypothesis, much of the UbCLaNt::R26CreERT2 mice phenotypes resemble those from mice where LM networks cannot form due either to LN domain mutations or overexpression of the LM-network disrupting protein, netrin-4. Specifically, mice with a mutation in the LN domain of LM α5 die before birth exhibiting defective lung development and vascular abnormalities in the kidneys [68]. While mice with LM β2 LN domain mutations or LN domain deletions exhibit renal defects, and although viable at birth, become progressively weaker and die between postnatal day 15 and 30 [69-74]. Additionally, mice with netrin-4 overexpression under the control of the K14 promoter were born smaller, redder, and with increased lymphatic permeability [35]. In comparison to each of these lines, the LaNt α31 animals present with similar but more severe and more widespread phenotypes, which reflects the more widespread UBC and R26 promoter activities. Nevertheless, based on the broad similarity between these phenotypes, we propose a model where LaNt α31 overexpression inhibits LM network assembly by competing with the native LM α chain. However, within this model, there remains the question of how LaNt α31 influences tissues where there the expressed LMs do not contain an α LN domain, and

bioRxiv preprint doi: https://doi.org/10.1101/2020.07.26.221663; this version posted November 24, 2020. The copyright holder for this preprint (which was not certified by peer review) is the author/funder, who has granted bioRxiv a license to display the preprint in perpetuity. It is made available under aCC-BY-NC 4.0 International license.

therefore are not able to polymerise [16]. For example, The LM composition present within vessel BMs during development and lymph vessels is rich in the β and γ LN domain-containing LM411 [75-77]. Here, one might have anticipated that the LaNt α31 LN domain could stabilise weak βγ LN dimers strengthening the BM but the observed phenotype of blood exudate throughout the mouse tissues suggests instead that the LaNt α31 transgenics have vascular leakage which overall points to a disruptive rather than stabilising role.

The in vivo findings here combined with previous in vitro studies support LaNt α31 acting as a regulator of BM homeostasis; however, we cannot yet fully rule out the possibility of LaNt α31 acting as a signalling protein [25, 37, 39, 40]. Specifically, integrin-mediated signalling from LaNt α31-like proteolytically released LN-domain containing fragments from LM α3b, α1, and β1 chains have been reported [27-29] and some aspects of the UbCLaNt::R26CreERT2 phenotype are consistent with LaNt α31 acting in this way. For example one of the most striking phenotypes observed in the UbCLaNt::R26CreERT2 mice was the depletion of hematopoietic colonies in the liver, an essential stem cell niche during development [78-80]. Integrins α6 and β1 are highly expressed in hematopoietic stem cells, and are central to the process of migration both in and out of the fetal liver [81-83], and a netrin-4/laminin γ1 complex has been shown to signal through the integrin α6β1 receptor [84]. Indeed, LaNt α31 may signal in a similar manner, which may be detrimental to the maintenance of hematopoietic colonies in the fetal liver. Moreover, we previously identified that LaNt α31 is enriched in human and porcine limbal stem cell niche of adult corneas, with expression further upregulated upon ex vivo stem cell activation and wound repair [37]. Coupled to the striking phenotype observed here, it is tempting to hypothesise that LaNt α31 is involved in regulating stem cell quiescence. While direct signaling effects could explain that role, indirect effects are also possible as altering LM network structural organisation changes outside-in signalling, through changing the presentation of ligands and by modifying growth factor sequestration and release rates [85]. Indeed, LM networks are critical for maintaining progenitor cell “stemness” [86-89]. Dissecting the direct versus indirect roles of LaNt α31 in intact tissue contexts is now a priority and the new transgenic line provides a valuable resource to facilitate those onward investigations.

bioRxiv preprint doi: https://doi.org/10.1101/2020.07.26.221663; this version posted November 24, 2020. The copyright holder for this preprint (which was not certified by peer review) is the author/funder, who has granted bioRxiv a license to display the preprint in perpetuity. It is made available under aCC-BY-NC 4.0 International license.

Moving forward, the role of LaNt α31 can now be determined in a tissue and context specific manner. In this study, we focused on widespread developmental expression as a BM formation and remodelling is highly active, thereby maximising the likelihood of determining whether LaNt α31 is functional in vivo and to focus future studies upon the most relevant tissues. Considering the widespread expression of LaNt α31[38], and the dramatic effects observed in this study, it is now important to determine effects in adult animals in normal conditions and following intervention. These studies should also include tissues where no overt LaNt α31-induced phenotype was observed. For example, although we did not observe muscle effects in these animals, LM network integrity is critical to muscle function, with the effects of LM α2 LN domain mutations or deletions developing muscular dystrophy and peripheral neuropathy with time [90-92], therefore, longer-term studies may reveal further phenotypes once tissues are placed under stress. As the LaNt α31 phenotypes are deleterious, further studies will require lineage-specific expression to gain deeper cellular and temporal resolution.

This study provides the first in vivo evidence that LaNt α31, the newest member of the LM superfamily, is a biologically relevant matricellular protein and emphasises the importance of α LN domains as regulators of tissue homeostasis. Indeed, whereas identification of α LN domain mutations in rare inherited disorders have established that LN domains matter [19, 22, 93-95], the LaNt α31 protein is a naturally occurring splice isoform [25] which suggests active regulation of the LN domain interactions *via* alternative splicing. Changes to alternative splicing rates often occur in normal situations, including during development and tissue remodelling, in response to damage such as in wound repair, and can be dysregulated in pathological situations including frequently in cancer [96-98] Considered in this way, the finding the LaNt α31 is biologically active in vivo has exciting and far-reaching implications for our understanding of BM biology.

bioRxiv preprint doi: https://doi.org/10.1101/2020.07.26.221663; this version posted November 24, 2020. The copyright holder for this preprint (which was not certified by peer review) is the author/funder, who has granted bioRxiv a license to display the preprint in perpetuity. It is made available under aCC-BY-NC 4.0 International license.

Acknowledgements

We are grateful to the staff at the University of Liverpool Biomedical Services Unit. We would like to thank Dr. Takao Sakai, Dr. Rachel Lennon, and Dr. Mychel Morais for helpful discussions during the writing of this manuscript.

Competing interests

No competing interests declared

Author contributions:

Conor J. Sugden: Methodology, Validation, Formal analysis, Investigation, Data Curation, Writing - Original Draft, Writing - Review & Editing, Visualization. **Valentina Iorio:** Methodology, Investigation, Data Curation, Writing - Review & Editing. **Lee D. Troughton:** Methodology, Writing - Original Draft, Writing - Review & Editing. **Ke Liu:** Methodology, Writing - Review & Editing. **George Bou-Gharios:** Conceptualization, Methodology, Writing - Review & Editing, Supervision. **Kevin Hamill:** Conceptualization, Methodology, Writing - Original Draft , Writing - Review & Editing, Supervision, Funding acquisition.

Funding

This work was supported by the biotechnology and biological sciences research council [grant number BB/L020513/1] and the The University of Liverpool Crossley Barnes Bequest fund.

bioRxiv preprint doi: https://doi.org/10.1101/2020.07.26.221663; this version posted November 24, 2020. The copyright holder for this preprint (which was not certified by peer review) is the author/funder, who has granted bioRxiv a license to display the preprint in perpetuity. It is made available under aCC-BY-NC 4.0 International license.

bioRxiv preprint doi: https://doi.org/10.1101/2020.07.26.221663; this version posted November 24, 2020. The copyright holder for this preprint (which was not certified by peer review) is the author/funder, who has granted bioRxiv a license to display the preprint in perpetuity. It is made available under aCC-BY-NC 4.0 International license.

References

1. Yamada KM, Collins JW, Cruz Walma DA, et al. Extracellular matrix dynamics in cell migration, invasion and tissue morphogenesis. *Int J Exp Pathol*. Jun 2019;100(3):144-152. doi:10.1111/iep.12329
2. Sekiguchi R, Yamada KM. Basement Membranes in Development and Disease. *Curr Top Dev Biol*. 2018;130:143-191. doi:10.1016/bs.ctdb.2018.02.005
3. Yurchenco PD. Basement membranes: cell scaffoldings and signaling platforms. *Cold Spring Harb Perspect Biol*. Feb 1 2011;3(2)doi:10.1101/cshperspect.a004911
4. Pozzi A, Yurchenco PD, Iozzo RV. The nature and biology of basement membranes. *Matrix Biol*. Jan 2017;57-58:1-11. doi:10.1016/j.matbio.2016.12.009
5. Walma DAC, Yamada KM. The extracellular matrix in development. *Development*. May 28 2020;147(10)doi:10.1242/dev.175596
6. Morrissey MA, Sherwood DR. An active role for basement membrane assembly and modification in tissue sculpting. *J Cell Sci*. May 1 2015;128(9):1661-8. doi:10.1242/jcs.168021
7. Theocharis AD, Skandalis SS, Gialeli C, Karamanos NK. Extracellular matrix structure. *Adv Drug Deliv Rev*. Feb 1 2016;97:4-27. doi:10.1016/j.addr.2015.11.001
8. Hamill KJ, Kligys K, Hopkinson SB, Jones JC. Laminin deposition in the extracellular matrix: a complex picture emerges. Research Support, N.I.H., Extramural. *J Cell Sci*. Dec 15 2009;122(Pt 24):4409-17. doi:10.1242/jcs.041095
9. Hohenester E, Yurchenco PD. Laminins in basement membrane assembly. Research Support, N.I.H., Extramural
Research Support, Non-U.S. Gov't
Review. *Cell adhesion & migration*. Jan-Feb 2013;7(1):56-63. doi:10.4161/cam.21831
10. Aumailley M. The laminin family. *Cell Adh Migr*. Jan-Feb 2013;7(1):48-55. doi:10.4161/cam.22826
11. Aumailley M, Bruckner-Tuderman L, Carter WG, et al. A simplified laminin nomenclature. *Matrix Biol*. Aug 2005;24(5):326-32. doi:10.1016/j.matbio.2005.05.006
12. Cheng YS, Champliaud MF, Burgeson RE, Marinkovich MP, Yurchenco PD. Self-assembly of laminin isoforms. *J Biol Chem*. Dec 12 1997;272(50):31525-32.
13. Odenthal U, Haehn S, Tunggal P, et al. Molecular analysis of laminin N-terminal domains mediating self-interactions. *J Biol Chem*. Oct 22 2004;279(43):44504-12. doi:10.1074/jbc.M402455200
14. Schittny JC, Yurchenco PD. Terminal short arm domains of basement membrane laminin are critical for its self-assembly. Research Support, Non-U.S. Gov't
Research Support, U.S. Gov't, P.H.S. *J Cell Biol*. Mar 1990;110(3):825-32.
15. Yurchenco PD, Cheng YS. Laminin self-assembly: a three-arm interaction hypothesis for the formation of a network in basement membranes. *Contrib Nephrol*. 1994;107:47-56. doi:10.1159/000422960
16. Purvis A, Hohenester E. Laminin network formation studied by reconstitution of ternary nodes in solution. Research Support, Non-U.S. Gov't. *J Biol Chem*. Dec 28 2012;287(53):44270-7. doi:10.1074/jbc.M112.418426

bioRxiv preprint doi: https://doi.org/10.1101/2020.07.26.221663; this version posted November 24, 2020. The copyright holder for this preprint (which was not certified by peer review) is the author/funder, who has granted bioRxiv a license to display the preprint in perpetuity. It is made available under aCC-BY-NC 4.0 International license.

17. Carafoli F, Hussain SA, Hohenester E. Crystal structures of the network-forming short-arm tips of the laminin beta1 and gamma1 chains. *PLoS One*. 2012;7(7):e42473. doi:10.1371/journal.pone.0042473

18. McKee KK, Aleksandrova M, Yurchenco PD. Chimeric protein identification of dystrophic, Pierson and other laminin polymerization residues. *Matrix Biol*. Apr 2018;67:32-46. doi:10.1016/j.matbio.2018.01.012

19. Matejas V, Hinkes B, Alkandari F, et al. Mutations in the human laminin beta2 (LAMB2) gene and the associated phenotypic spectrum. *Hum Mutat*. Sep 2010;31(9):992-1002. doi:10.1002/humu.21304

20. Funk SD, Lin MH, Miner JH. Alport syndrome and Pierson syndrome: Diseases of the glomerular basement membrane. *Matrix Biol*. Oct 2018;71-72:250-261. doi:10.1016/j.matbio.2018.04.008

21. Gawlik KI, Durbeej M. Skeletal muscle laminin and MDC1A: pathogenesis and treatment strategies. *Skelet Muscle*. Mar 1 2011;1(1):9. doi:10.1186/2044-5040-1-9

22. Funk SD, Bayer RH, Malone AF, McKee KK, Yurchenco PD, Miner JH. Pathogenicity of a Human Laminin beta2 Mutation Revealed in Models of Alport Syndrome. *J Am Soc Nephrol*. Mar 2018;29(3):949-960. doi:10.1681/ASN.2017090997

23. Hohenester E. Structural biology of laminins. *Essays Biochem*. Sep 13 2019;63(3):285-295. doi:10.1042/EBC20180075

24. Yousif LF, Di Russo J, Sorokin L. Laminin isoforms in endothelial and perivascular basement membranes. *Cell Adh Migr*. Jan-Feb 2013;7(1):101-10. doi:10.4161/cam.22680

25. Hamill KJ, Langbein L, Jones JC, McLean WH. Identification of a novel family of laminin N-terminal alternate splice isoforms: structural and functional characterization. *J Biol Chem*. Dec 18 2009;284(51):35588-96. doi:10.1074/jbc.M109.052811

26. Rajasekharan S, Kennedy TE. The netrin protein family. *Genome biology*. 2009;10(9):239. doi:gb-2009-10-9-239 [pii] 10.1186/gb-2009-10-9-239

27. Ettner N, Gohring W, Sasaki T, Mann K, Timpl R. The N-terminal globular domain of the laminin alpha1 chain binds to alpha1beta1 and alpha2beta1 integrins and to the heparan sulfate-containing domains of perlecan. *FEBS Lett*. Jul 3 1998;430(3):217-21. doi:10.1016/s0014-5793(98)00601-2

28. Horejs CM, Serio A, Purvis A, et al. Biologically-active laminin-111 fragment that modulates the epithelial-to-mesenchymal transition in embryonic stem cells. *Proc Natl Acad Sci U S A*. Apr 22 2014;111(16):5908-13. doi:10.1073/pnas.1403139111

29. Kariya Y, Yasuda C, Nakashima Y, Ishida K, Tsubota Y, Miyazaki K. Characterization of laminin 5B and NH2-terminal proteolytic fragment of its alpha3B chain: promotion of cellular adhesion, migration, and proliferation. *J Biol Chem*. Jun 4 2004;279(23):24774-84. doi:10.1074/jbc.M400670200

30. Lai Wing Sun K, Correia JP, Kennedy TE. Netrins: versatile extracellular cues with diverse functions. *Development*. Jun 2011;138(11):2153-69. doi:10.1242/dev.044529

31. Fahey B, Degnan BM. Origin and evolution of laminin gene family diversity. *Mol Biol Evol*. Jul 2012;29(7):1823-36. doi:10.1093/molbev/mss060

32. Leclere L, Rentzsch F. Repeated evolution of identical domain architecture in metazoan netrin domain-containing proteins. *Genome Biol Evol*. 2012;4(9):883-99. doi:10.1093/gbe/evs061

bioRxiv preprint doi: https://doi.org/10.1101/2020.07.26.221663; this version posted November 24, 2020. The copyright holder for this preprint (which was not certified by peer review) is the author/funder, who has granted bioRxiv a license to display the preprint in perpetuity. It is made available under aCC-BY-NC 4.0 International license.

33. Reuten R, Patel TR, McDougall M, et al. Structural decoding of netrin-4 reveals a regulatory function towards mature basement membranes. *Nat Commun*. Nov 30 2016;7:13515. doi:10.1038/ncomms13515

34. Schneiders FI, Maertens B, Bose K, et al. Binding of netrin-4 to laminin short arms regulates basement membrane assembly. *J Biol Chem*. Aug 17 2007;282(33):23750-8. doi:10.1074/jbc.M703137200

35. Larrieu-Lahargue F, Welm AL, Thomas KR, Li DY. Netrin-4 induces lymphangiogenesis in vivo. *Blood*. Jul 1 2010;115(26):5418-26. doi:10.1182/blood-2009-11-252338

36. Koch M, Murrell JR, Hunter DD, et al. A novel member of the netrin family, beta-netrin, shares homology with the beta chain of laminin: identification, expression, and functional characterization. *J Cell Biol*. Oct 16 2000;151(2):221-34. doi:10.1083/jcb.151.2.221

37. Barrera V, Troughton LD, Iorio V, et al. Differential Distribution of Laminin N-Terminus alpha31 Across the Ocular Surface: Implications for Corneal Wound Repair. *Invest Ophthalmol Vis Sci*. Aug 1 2018;59(10):4082-4093. doi:10.1167/iovs.18-24037

38. Troughton LD, Reuten R, Sugden CJ, Hamill KJ. Laminin N-terminus α31 protein distribution in adult human tissues. *bioRxiv*. 2020:2020.05.21.108134. doi:10.1101/2020.05.21.108134

39. Troughton LD, Zech T, Hamill KJ. Laminin N-terminus α31 is upregulated in invasive ductal breast cancer and changes the mode of tumour invasion. *bioRxiv*. 2020:2020.05.28.120964. doi:10.1101/2020.05.28.120964

40. Iorio V, Troughton LD, Barrera V, Hamill KJ. LaNt α31 modulates LM332 organisation during matrix deposition leading to cell-matrix adhesion and migration defects. *bioRxiv*. 2019:617597. doi:10.1101/617597

41. Pribnow D. Nucleotide sequence of an RNA polymerase binding site at an early T7 promoter. *Proc Natl Acad Sci U S A*. Mar 1975;72(3):784-8. doi:10.1073/pnas.72.3.784

42. Kozak M. An analysis of 5'-noncoding sequences from 699 vertebrate messenger RNAs. *Nucleic Acids Res*. Oct 26 1987;15(20):8125-48. doi:10.1093/nar/15.20.8125

43. Coloma MJ, Hastings A, Wims LA, Morrison SL. Novel vectors for the expression of antibody molecules using variable regions generated by polymerase chain reaction. *J Immunol Methods*. Jul 31 1992;152(1):89-104. doi:10.1016/0022-1759(92)90092-8

44. Brizzard BL, Chubet RG, Vizard DL. Immunoaffinity purification of FLAG epitope-tagged bacterial alkaline phosphatase using a novel monoclonal antibody and peptide elution. *Biotechniques*. Apr 1994;16(4):730-5.

45. Field J, Nikawa J, Broek D, et al. Purification of a RAS-responsive adenylyl cyclase complex from Saccharomyces cerevisiae by use of an epitope addition method. *Mol Cell Biol*. May 1988;8(5):2159-65. doi:10.1128/mcb.8.5.2159

46. Kim JH, Lee SR, Li LH, et al. High cleavage efficiency of a 2A peptide derived from porcine teschovirus-1 in human cell lines, zebrafish and mice. *PLoS One*. 2011;6(4):e18556. doi:10.1371/journal.pone.0018556

47. Yuspa SH, Harris CC. Altered differentiation of mouse epidermal cells treated with retinyl acetate in vitro. *Exp Cell Res*. May 1974;86(1):95-105. doi:10.1016/0014-4827(74)90653-3

48. Ittner LM, Gotz J. Pronuclear injection for the production of transgenic mice. *Nat Protoc*. 2007;2(5):1206-15. doi:10.1038/nprot.2007.145

bioRxiv preprint doi: https://doi.org/10.1101/2020.07.26.221663; this version posted November 24, 2020. The copyright holder for this preprint (which was not certified by peer review) is the author/funder, who has granted bioRxiv a license to display the preprint in perpetuity. It is made available under aCC-BY-NC 4.0 International license.

49. Ventura A, Kirsch DG, McLaughlin ME, et al. Restoration of p53 function leads to tumour regression in vivo. *Nature*. Feb 8 2007;445(7128):661-5. doi:10.1038/nature05541

50. Schneider CA, Rasband WS, Eliceiri KW. NIH Image to ImageJ: 25 years of image analysis. *Nat Methods*. Jul 2012;9(7):671-5. doi:10.1038/nmeth.2089

51. Schmidt U, Weigert M, Broaddus C, Myers G. Cell Detection with Star-Convex Polygons. Springer International Publishing; 2018:265-273.

52. Ochiai H, Harashima H, Kamiya H. Effects of insulator cHS4 on transgene expression from plasmid DNA in a positive feedback system. *J Biosci Bioeng*. Nov 2011;112(5):432-4. doi:10.1016/j.jbiosc.2011.07.001

53. Zenker M, Aigner T, Wendler O, et al. Human laminin beta2 deficiency causes congenital nephrosis with mesangial sclerosis and distinct eye abnormalities. *Hum Mol Genet*. Nov 1 2004;13(21):2625-32. doi:10.1093/hmg/ddh284

54. Zenker M, Pierson M, Jonveaux P, Reis A. Demonstration of two novel LAMB2 mutations in the original Pierson syndrome family reported 42 years ago. *Am J Med Genet A*. Sep 15 2005;138(1):73-4. doi:10.1002/ajmg.a.30894

55. Hinkes BG, Mucha B, Vlangos CN, et al. Nephrotic syndrome in the first year of life: two thirds of cases are caused by mutations in 4 genes (NPHS1, NPHS2, WT1, and LAMB2). *Pediatrics*. Apr 2007;119(4):e907-19. doi:10.1542/peds.2006-2164

56. Chen YM, Kikkawa Y, Miner JH. A missense LAMB2 mutation causes congenital nephrotic syndrome by impairing laminin secretion. *J Am Soc Nephrol*. May 2011;22(5):849-58. doi:10.1681/ASN.2010060632

57. Kiritsi D, Has C, Bruckner-Tuderman L. Laminin 332 in junctional epidermolysis bullosa. *Cell Adh Migr*. Jan-Feb 2013;7(1):135-41. doi:10.4161/cam.22418

58. McLean WH, Irvine AD, Hamill KJ, et al. An unusual N-terminal deletion of the laminin alpha3a isoform leads to the chronic granulation tissue disorder laryngo-onycho-cutaneous syndrome. *Hum Mol Genet*. Sep 15 2003;12(18):2395-409. doi:10.1093/hmg/ddg234

59. Barzegar M, Mozafari N, Kariminejad A, Asadikani Z, Ozoemena L, McGrath JA. A new homozygous nonsense mutation in LAMA3A underlying laryngo-onycho-cutaneous syndrome. *Br J Dermatol*. Dec 2013;169(6):1353-6. doi:10.1111/bjd.12522

60. Pierce RA, Griffin GL, Mudd MS, et al. Expression of laminin alpha3, alpha4, and alpha5 chains by alveolar epithelial cells and fibroblasts. *Am J Respir Cell Mol Biol*. Aug 1998;19(2):237-44. doi:10.1165/ajrcmb.19.2.3087

61. DeBiase PJ, Lane K, Budinger S, Ridge K, Wilson M, Jones JC. Laminin-311 (Laminin-6) fiber assembly by type I-like alveolar cells. *J Histochem Cytochem*. Jun 2006;54(6):665-72. doi:10.1369/jhc.5A6889.2006

62. Morales-Nebreda LI, Rogel MR, Eisenberg JL, et al. Lung-specific loss of alpha3 laminin worsens bleomycin-induced pulmonary fibrosis. *Am J Respir Cell Mol Biol*. Apr 2015;52(4):503-12. doi:10.1165/rcmb.2014-0057OC

63. Coulombe PA, Kopan R, Fuchs E. Expression of keratin K14 in the epidermis and hair follicle: insights into complex programs of differentiation. *J Cell Biol*. Nov 1989;109(5):2295-312. doi:10.1083/jcb.109.5.2295

64. Vasioukhin V, Degenstein L, Wise B, Fuchs E. The magical touch: genome targeting in epidermal stem cells induced by tamoxifen application to mouse skin. *Proc Natl Acad Sci U S A*. Jul 20 1999;96(15):8551-6. doi:10.1073/pnas.96.15.8551

bioRxiv preprint doi: https://doi.org/10.1101/2020.07.26.221663; this version posted November 24, 2020. The copyright holder for this preprint (which was not certified by peer review) is the author/funder, who has granted bioRxiv a license to display the preprint in perpetuity. It is made available under aCC-BY-NC 4.0 International license.

65. Wang X, Zinkel S, Polonsky K, Fuchs E. Transgenic studies with a keratin promoter-driven growth hormone transgene: prospects for gene therapy. *Proc Natl Acad Sci U S A*. Jan 7 1997;94(1):219-26. doi:10.1073/pnas.94.1.219

66. Hafner M, Wenk J, Nenci A, et al. Keratin 14 Cre transgenic mice authenticate keratin 14 as an oocyte-expressed protein. *Genesis*. Apr 2004;38(4):176-81. doi:10.1002/gene.20016

67. Hussain SA, Carafoli F, Hohenester E. Determinants of laminin polymerization revealed by the structure of the alpha5 chain amino-terminal region. *EMBO Rep*. Mar 2011;12(3):276-82. doi:10.1038/embor.2011.3

68. Jones LK, Lam R, McKee KK, et al. A mutation affecting laminin alpha 5 polymerisation gives rise to a syndromic developmental disorder. *Development*. May 21 2020;doi:10.1242/dev.189183

69. Noakes PG, Gautam M, Mudd J, Sanes JR, Merlie JP. Aberrant differentiation of neuromuscular junctions in mice lacking s-laminin/laminin beta 2. *Nature*. Mar 16 1995;374(6519):258-62. doi:10.1038/374258a0

70. Noakes PG, Miner JH, Gautam M, Cunningham JM, Sanes JR, Merlie JP. The renal glomerulus of mice lacking s-laminin/laminin beta 2: nephrosis despite molecular compensation by laminin beta 1. *Nat Genet*. Aug 1995;10(4):400-6. doi:10.1038/ng0895-400

71. Miner JH, Go G, Cunningham J, Patton BL, Jarad G. Transgenic isolation of skeletal muscle and kidney defects in laminin beta2 mutant mice: implications for Pierson syndrome. *Development*. Mar 2006;133(5):967-75. doi:10.1242/dev.02270

72. Jarad G, Cunningham J, Shaw AS, Miner JH. Proteinuria precedes podocyte abnormalities inLamb2-/- mice, implicating the glomerular basement membrane as an albumin barrier. *J Clin Invest*. Aug 2006;116(8):2272-9. doi:10.1172/JCI28414

73. Libby RT, Lavallee CR, Balkema GW, Brunken WJ, Hunter DD. Disruption of laminin beta2 chain production causes alterations in morphology and function in the CNS. *J Neurosci*. Nov 1 1999;19(21):9399-411.

74. Denes V, Witkovsky P, Koch M, Hunter DD, Pinzon-Duarte G, Brunken WJ. Laminin deficits induce alterations in the development of dopaminergic neurons in the mouse retina. *Vis Neurosci*. Jul-Aug 2007;24(4):549-62. doi:10.1017/S0952523807070514

75. Hallmann R, Horn N, Selg M, Wendler O, Pausch F, Sorokin LM. Expression and function of laminins in the embryonic and mature vasculature. *Physiol Rev*. Jul 2005;85(3):979-1000. doi:10.1152/physrev.00014.2004

76. Petajaniemi N, Korhonen M, Kortesmaa J, et al. Localization of laminin alpha4-chain in developing and adult human tissues. *J Histochem Cytochem*. Aug 2002;50(8):1113-30. doi:10.1177/002215540205000813

77. Vainionpaa N, Butzow R, Hukkanen M, et al. Basement membrane protein distribution in LYVE-1-immunoreactive lymphatic vessels of normal tissues and ovarian carcinomas. *Cell Tissue Res*. May 2007;328(2):317-28. doi:10.1007/s00441-006-0366-2

78. Moore MA, Metcalf D. Ontogeny of the haemopoietic system: yolk sac origin of in vivo and in vitro colony forming cells in the developing mouse embryo. *Br J Haematol*. Mar 1970;18(3):279-96. doi:10.1111/j.1365-2141.1970.tb01443.x

79. Sanchez MJ, Holmes A, Miles C, Dzierzak E. Characterization of the first definitive hematopoietic stem cells in the AGM and liver of the mouse embryo. *Immunity*. Dec 1996;5(6):513-25. doi:10.1016/s1074-7613(00)80267-8

80. Dzierzak E, Speck NA. Of lineage and legacy: the development of mammalian hematopoietic stem cells. *Nat Immunol*. Feb 2008;9(2):129-36. doi:10.1038/ni1560

bioRxiv preprint doi: https://doi.org/10.1101/2020.07.26.221663; this version posted November 24, 2020. The copyright holder for this preprint (which was not certified by peer review) is the author/funder, who has granted bioRxiv a license to display the preprint in perpetuity. It is made available under aCC-BY-NC 4.0 International license.

81. Qian H, Tryggvason K, Jacobsen SE, Ekblom M. Contribution of alpha6 integrins to hematopoietic stem and progenitor cell homing to bone marrow and collaboration with alpha4 integrins. *Blood*. May 1 2006;107(9):3503-10. doi:10.1182/blood-2005-10-3932

82. Potocnik AJ, Brakebusch C, Fassler R. Fetal and adult hematopoietic stem cells require beta1 integrin function for colonizing fetal liver, spleen, and bone marrow. *Immunity*. Jun 2000;12(6):653-63. doi:10.1016/s1074-7613(00)80216-2

83. Hirsch E, Iglesias A, Potocnik AJ, Hartmann U, Fassler R. Impaired migration but not differentiation of haematopoietic stem cells in the absence of beta1 integrins. *Nature*. Mar 14 1996;380(6570):171-5. doi:10.1038/380171a0

84. Staquicini FI, Dias-Neto E, Li J, et al. Discovery of a functional protein complex of netrin-4, laminin gamma1 chain, and integrin alpha6beta1 in mouse neural stem cells. *Proc Natl Acad Sci U S A*. Feb 24 2009;106(8):2903-8. doi:10.1073/pnas.0813286106

85. Sher I, Zisman-Rozen S, Eliahu L, et al. Targeting perlecan in human keratinocytes reveals novel roles for perlecan in epidermal formation. *J Biol Chem*. Feb 24 2006;281(8):5178-87. doi:10.1074/jbc.M509500200

86. Penton CM, Badarinarayana V, Prisco J, et al. Laminin 521 maintains differentiation potential of mouse and human satellite cell-derived myoblasts during long-term culture expansion. *Skelet Muscle*. Dec 13 2016;6(1):44. doi:10.1186/s13395-016-0116-4

87. Kiyozumi D, Nakano I, Sato-Nishiuchi R, Tanaka S, Sekiguchi K. Laminin is the ECM niche for trophoblast stem cells. *Life Sci Alliance*. Feb 2020;3(2)doi:10.26508/lsa.201900515

88. Rodin S, Domogatskaya A, Strom S, et al. Long-term self-renewal of human pluripotent stem cells on human recombinant laminin-511. *Nat Biotechnol*. Jun 2010;28(6):611-5. doi:10.1038/nbt.1620

89. Polisetti N, Sorokin L, Okumura N, et al. Laminin-511 and -521-based matrices for efficient ex vivo-expansion of human limbal epithelial progenitor cells. *Sci Rep*. Jul 11 2017;7(1):5152. doi:10.1038/s41598-017-04916-x

90. Sunada Y, Bernier SM, Utani A, Yamada Y, Campbell KP. Identification of a novel mutant transcript of laminin alpha 2 chain gene responsible for muscular dystrophy and dysmyelination in dy2J mice. *Hum Mol Genet*. Jun 1995;4(6):1055-61. doi:10.1093/hmg/4.6.1055

91. Xu H, Wu XR, Wewer UM, Engvall E. Murine muscular dystrophy caused by a mutation in the laminin alpha 2 (Lama2) gene. *Nat Genet*. Nov 1994;8(3):297-302. doi:10.1038/ng1194-297

92. Payne S, De Val S, Neal A. Endothelial-Specific Cre Mouse Models. *Arterioscler Thromb Vasc Biol*. Nov 2018;38(11):2550-2561. doi:10.1161/ATVBAHA.118.309669

93. Jones LK, Lam R, McKee KK, et al. A mutation affecting laminin alpha 5 polymerisation gives rise to a syndromic developmental disorder. *Development*. Jun 22 2020;147(21)doi:10.1242/dev.189183

94. Patton BL, Wang B, Tarumi YS, Seburn KL, Burgess RW. A single point mutation in the LN domain of LAMA2 causes muscular dystrophy and peripheral amyelination. *J Cell Sci*. May 15 2008;121(Pt 10):1593-604. doi:10.1242/jcs.015354

95. Yurchenco PD, McKee KK, Reinhard JR, Ruegg MA. Laminin-deficient muscular dystrophy: Molecular pathogenesis and structural repair strategies. *Matrix Biol*. Oct 2018;71-72:174-187. doi:10.1016/j.matbio.2017.11.009

bioRxiv preprint doi: https://doi.org/10.1101/2020.07.26.221663; this version posted November 24, 2020. The copyright holder for this preprint (which was not certified by peer review) is the author/funder, who has granted bioRxiv a license to display the preprint in perpetuity. It is made available under aCC-BY-NC 4.0 International license.

96. Poulos MG, Batra R, Charizanis K, Swanson MS. Developments in RNA splicing and disease. *Cold Spring Harb Perspect Biol*. Jan 1 2011;3(1):a000778. doi:10.1101/cshperspect.a000778

97. Baralle FE, Giudice J. Alternative splicing as a regulator of development and tissue identity. *Nat Rev Mol Cell Biol*. Jul 2017;18(7):437-451. doi:10.1038/nrm.2017.27

98. Ffrench-Constant C, Van de Water L, Dvorak HF, Hynes RO. Reappearance of an embryonic pattern of fibronectin splicing during wound healing in the adult rat. *J Cell Biol*. Aug 1989;109(2):903-14. doi:10.1083/jcb.109.2.903

bioRxiv preprint doi: https://doi.org/10.1101/2020.07.26.221663; this version posted November 24, 2020. The copyright holder for this preprint (which was not certified by peer review) is the author/funder, who has granted bioRxiv a license to display the preprint in perpetuity. It is made available under aCC-BY-NC 4.0 International license.

Figure legends

Figure 1 - Validation of UbCLaNt Cre-inducible construct in vitro

A) Diagram of the pUbC-LoxP-LaNt-α31-T2A-tdTomato construct. B) HEK 293A cells were transfected with pUbC-LoxP-LaNt-α31-T2A-tdTomato, pCAG-Cre:GFP, or pUbC-LoxP-LaNt-α31-T2A-tdTomato and pCAG-Cre:GFP and imaged 48 h after transfection. Scale bar 100 µm C) PCR was performed using primers flanking the stop cassette on DNA extracted from HEK293A cells co-transfected with pUbC-LoxP-LaNt-α31-T2A-tdTomato and pCAG-Cre:GFP. D) Western blot of lysates from HEK293 cells either untransfected or transfected with CMV- LaNt-α31-T2A-Dendra2 (positive control), or pUbC-LoxP-LaNt-α31-T2A-tdTomato and pCAG-Cre:GFP then probed with anti-flag antibodies

Figure 2 -UbC-LoxP-LaNt-α31-T2A-tdTomato embryonic fibroblast express the transgene upon transduction with a Cre recombinase-coding adenovirus

A) PCR was performed on gDNA of F1 UbC-LoxP-LaNt-α31-T2A-tdTomato embryos. B) Western blot of protein lysates from explanted F1 mouse embryonic fibroblasts processed with anti-HA antibodies. C) Fluorescence microscopy images of explanted cells from UbC-LoxP-LaNt-α31-T2A-tdTomato F1 mice. Scale bar = 100 µm.

Figure 3 - UbCLaNtα31 x R26CreERT2 ER transgenic mice express the UbC-LaNtα31 transgene following exposure to tamoxifen

A) Schematic diagram of the UbC-LaNt-α31 and Rosa-Cre transgenes. B) PCR performed using primers flanking the stop cassette on DNA extracted from transgenic mouse embryos from a UbCLaNtα31 x R26CreERT2 mating. C) Phase contrast and fluorescence microscopy images of explanted cells from UbCLaNtα31::R26CreERT2 embryos. Scale bar = 100 µm. D) Western blot of lysates from UbCLaNtα31::R26CreERT2 embryo explants processed with anti-HA antibodies.

bioRxiv preprint doi: https://doi.org/10.1101/2020.07.26.221663; this version posted November 24, 2020. The copyright holder for this preprint (which was not certified by peer review) is the author/funder, who has granted bioRxiv a license to display the preprint in perpetuity. It is made available under aCC-BY-NC 4.0 International license.

Figure 4 - Transgenic mice overexpressing LaNtα31 display localised regions of erythema

A) Representative images of UbCLaNt::R26CreERT2 P0 mice B) PCR genotyping of transgenic mice. C) Fluorescence microscopy images of explanted cells from UbCLaNt::R26CreERT2 P0 mice. D) Western blot of tissue lysates of UbCLaNt::R26CreERT2 P0 mice. E) Representative fluorescence microscopy UbCLaNt::R26CreERT2 P0 mouse OCT sections (8 μm) probed with anti-mCherry antibodies. Yellow arrows indicate cells expressing the tdTomato transgene reporter. Scale bar = 100 μm.

Figure 5 - LaNt α31 overexpression leads to epithelial detachment, tubular dilation and interstitial bleeding in the kidney and thickening of the tubular basement membrane.

A) Representative images of H&E stained FFPE sections (5 μm) of newborn UbCLaNt::R26CreERT2 transgenic mouse kidneys. Middle and right columns show areas of increased magnification. Black arrows point to areas of epithelial detachment. White arrows point to tubular dilation. Yellow arrows point to areas of interstitial bleeding. B) UbCLaNt::R26CreERT2 P0 mouse FFPE sections (5 μm) processed for immunohistochemistry with anti-laminin 111 polyclonal antibodies. Middle and right columns show areas of increased magnification. Scale bars = 100 μm.

Figure 6 - LaNt α31 overexpression disrupts epidermal-dermal basement membrane.

A) H&E staining of FFPE sections (5 μm) of newborn UbCLaNt::R26CreERT2 transgenic mouse dorsal skin. Middle and right columns show increased magnification of the epithelium or hair follicles respectively. Yellow arrows indicate basal layer of epithelial cells. Scale bar = 100 μm. B) UbCLaNt::R26CreERT2 P0 mouse FFPE sections (5 μm) processed for immunohistochemistry with anti-laminin 111 immunoreactivity. Middle and right columns show areas of increased magnification. Yellow arrows indicate the epidermal-dermal junction. Scale bar = 100 μm.

Figure 7 - Mice expressing the LaNtα31 transgene display structural differences in the lung and a reduction of hematopoietic colonies in the liver.

bioRxiv preprint doi: https://doi.org/10.1101/2020.07.26.221663; this version posted November 24, 2020. The copyright holder for this preprint (which was not certified by peer review) is the author/funder, who has granted bioRxiv a license to display the preprint in perpetuity. It is made available under aCC-BY-NC 4.0 International license.

A) UbCLaNtα31::R26CreERT2 P0 lung FFPE sections (5 μm) stained with H&E. Middle and right columns show areas of increased magnification. B) H&E staining of FFPE sections (5 μm) of newborn UbCLaNt::R26CreERT2 transgenic mouse skin. Middle and right columns show increased magnification of different area of the liver. Yellow arrowheads highlight areas of increased cell density. Scale bars = 100 μm. C) Representative image analysis method of determining nuclei count. D) Quantification of nuclei.

Supplemental Figure 1 – Transgenic expression of LaNt α31 under control of the human keratin-14 promoter results in a low number of offspring.

A) Diagram of the phK14-LaNtα31-T2A-mCherry construct. B) Fluorescence microscopy images of KERA 308 cells transfected with phK14-LaNtα31-T2A-mCherry. C) Western blot of protein lysates from transfected KERA 308 cells. D) Schematic of F0 mice generation and PCR genotyping of F0 mice. E) PCR genotyping of F1 mice. F) Representative fluorescence images of frozen sections from F1 mice tissues. G) Western blot of tissue lysates from F1 mice, probed with anti-His antibodies.

A

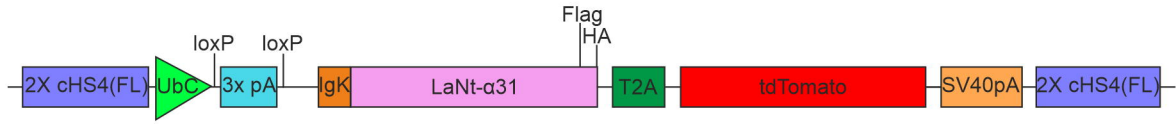
Flag
HA
loxP
loxP
2X cHS4(FL)
UbC
3x pA
IgK
LaNt-α31
T2A
tdTomato
SV40pA
2X cHS4(FL)

B

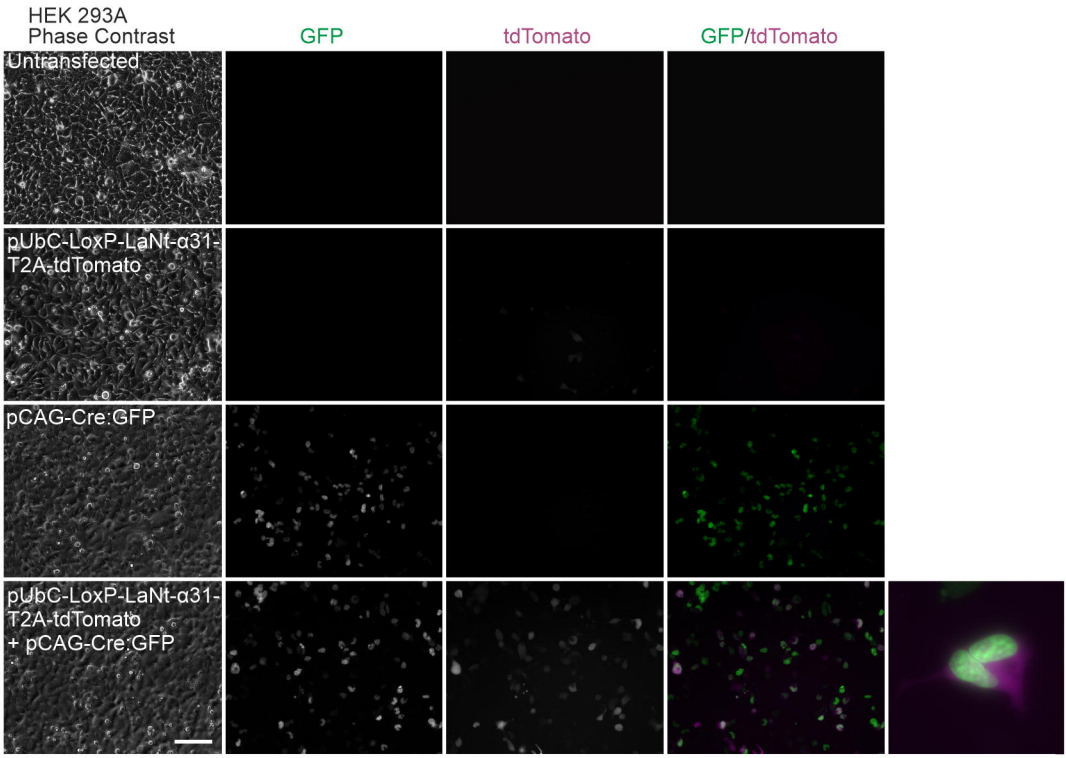
HEK 293A
Phase Contrast
GFP
tdTomato
GFP/tdTomato
Untransfected
pUbC-LoxP-LaNt-α31-T2A-tdTomato
pCAG-Cre:GFP
pUbC-LoxP-LaNt-α31-T2A-tdTomato + pCAG-Cre:GFP

C

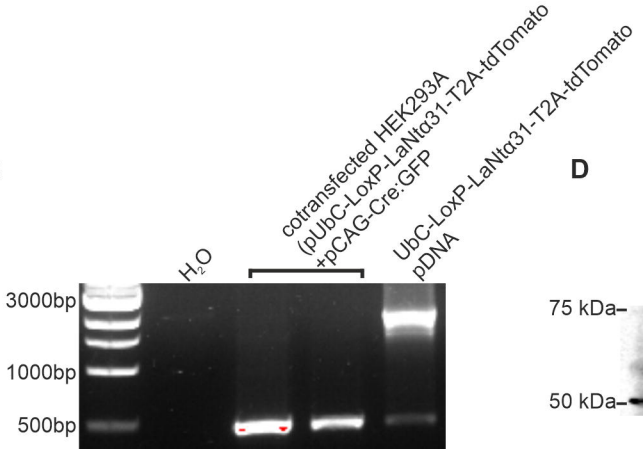
H2O
cotransfected HEK293A (pUbC-LoxP-LaNtα31-T2A-tdTomato +pCAG-Cre:GFP
UbC-LoxP-LaNtα31-T2A-tdTomato pDNA
3000bp
1000bp
500bp

D

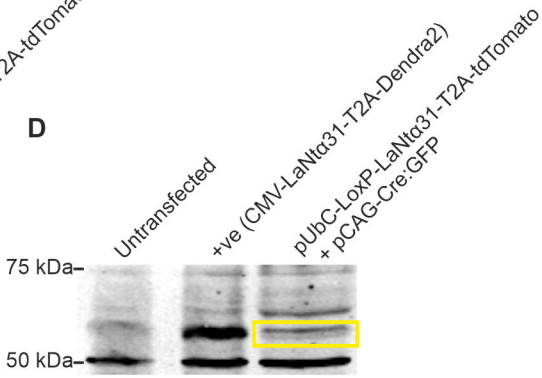
Untransfected
+ve (CMV-LaNtα31-T2A-Dendra2)
pUbC-LoxP-LaNtα31-T2A-tdTomato + pCAG-Cre:GFP
75 kDa
50 kDa

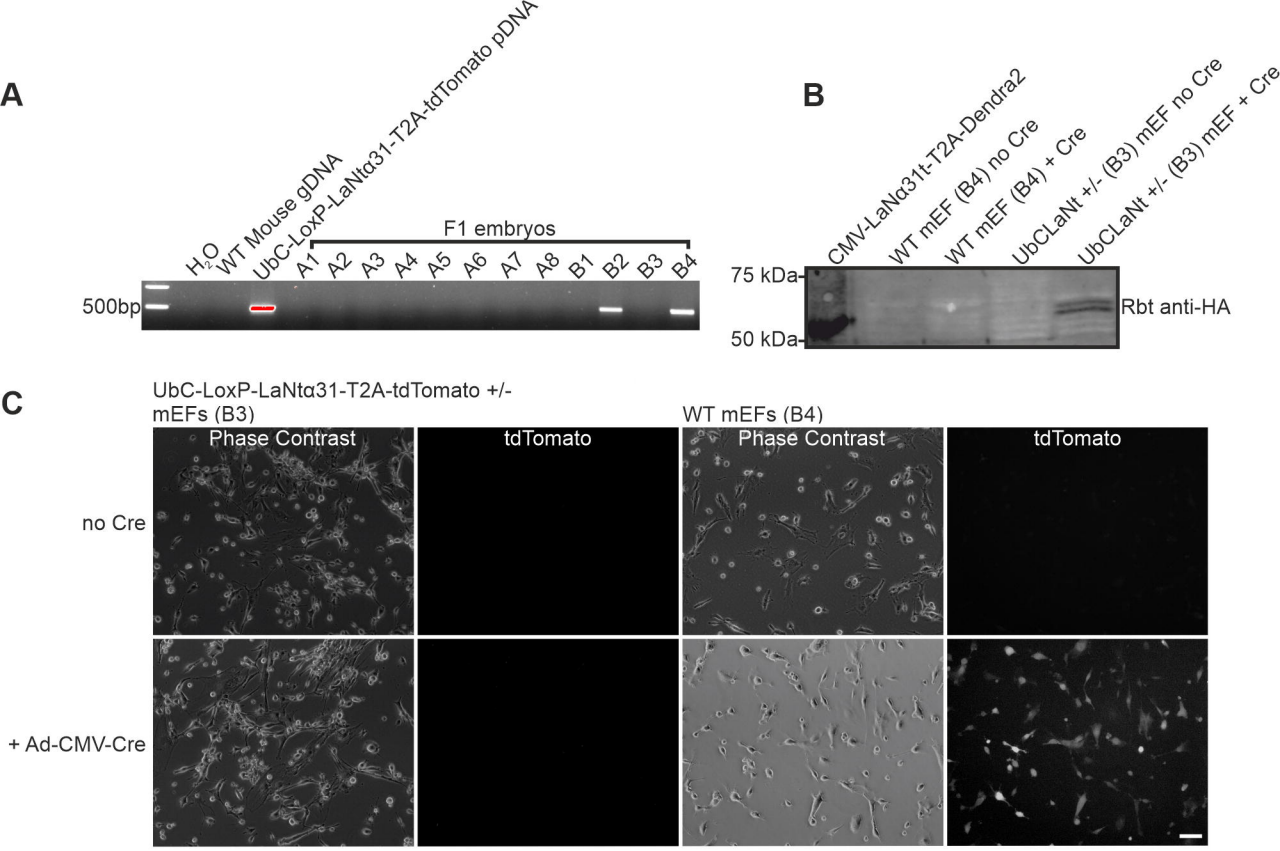
A
H2O
WT Mouse gDNA
UbC-LoxP-LaNtα31-T2A-tdTomato pDNA
F1 embryos
A1
A2
A3
A4
A5
A6
A7
A8
B1
B2
B3
B4
500bp
B
CMV-LaNtα31t-T2A-Dendra2
WT mEF (B4) no Cre
WT mEF (B4) + Cre
UbCLaNt +/- (B3) mEF no Cre
UbCLaNt +/- (B3) mEF + Cre
75 kDa
50 kDa
Rbt anti-HA
C
UbC-LoxP-LaNtα31-T2A-tdTomato +/- mEFs (B3)
WT mEFs (B4)
Phase Contrast
tdTomato
Phase Contrast
tdTomato
no Cre
+ Ad-CMV-Cre

A

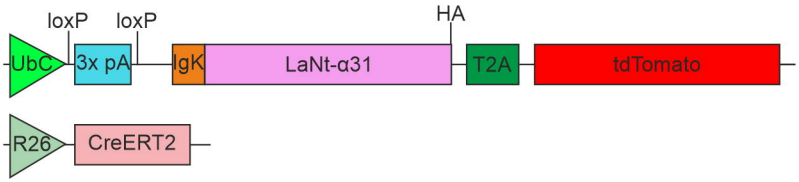
loxP
loxP
HA
UbC
3x pA
IgK
LaNt-α31
T2A
tdTomato
R26
CreERT2

B

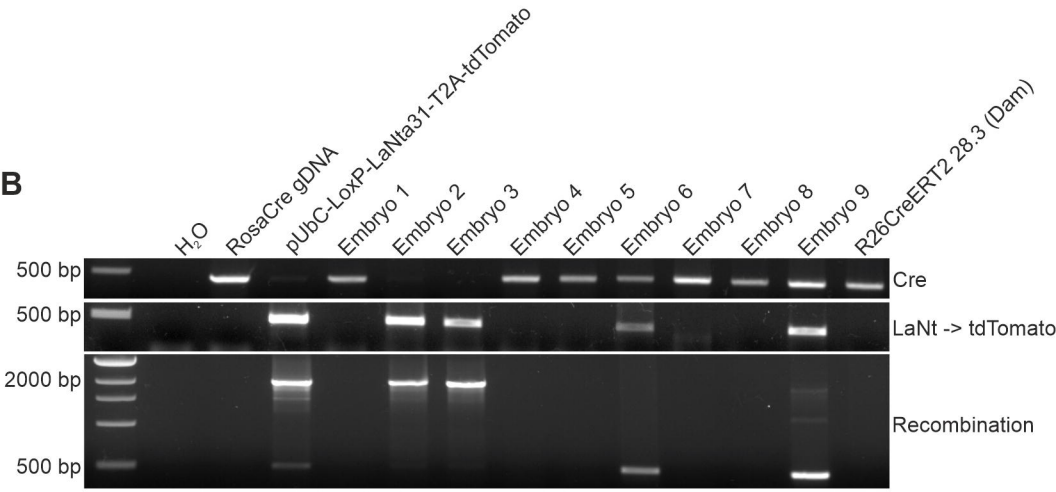
H2O
RosaCre gDNA
pUbC-LoxP-LaNta31-T2A-tdTomato
Embryo 1
Embryo 2
Embryo 3
Embryo 4
Embryo 5
Embryo 6
Embryo 7
Embryo 8
Embryo 9
R26CreERT2 28.3 (Dam)
500 bp
Cre
500 bp
LaNt -> tdTomato
2000 bp
Recombination
500 bp

C

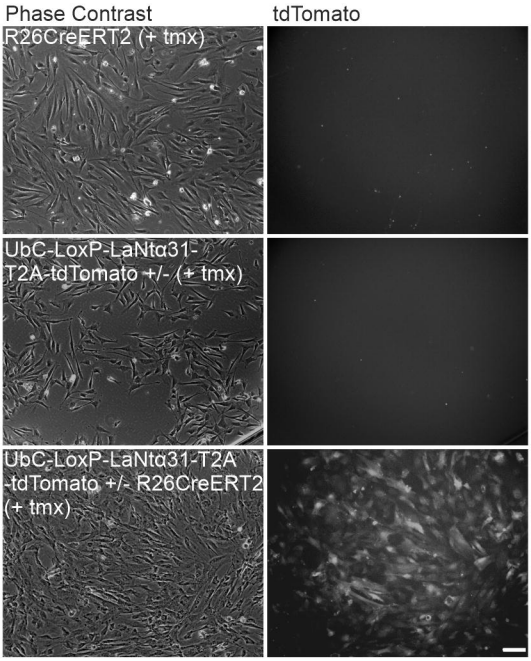
Phase Contrast
tdTomato
R26CreERT2 (+ tmx)
UbC-LoxP-LaNtα31-T2A-tdTomato +/- (+ tmx)
UbC-LoxP-LaNtα31-T2A -tdTomato +/- R26CreERT2 (+ tmx)

D

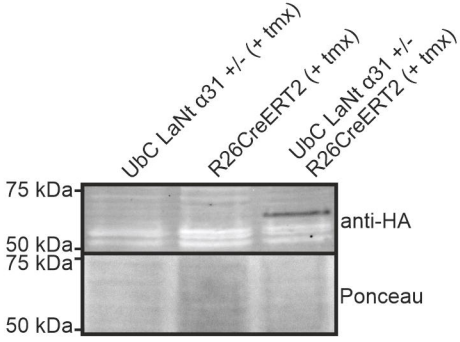
UbC LaNt α31 +/- (+ tmx)
R26CreERT2 (+ tmx)
UbC LaNt α31 +/- R26CreERT2 (+ tmx)
75 kDa
50 kDa
anti-HA
75 kDa
50 kDa
Ponceau

A

UbCLaNt::R26CreERT2 2NE2 non-expressing

UbCLaNt::R26CreERT2 2E1 expressing

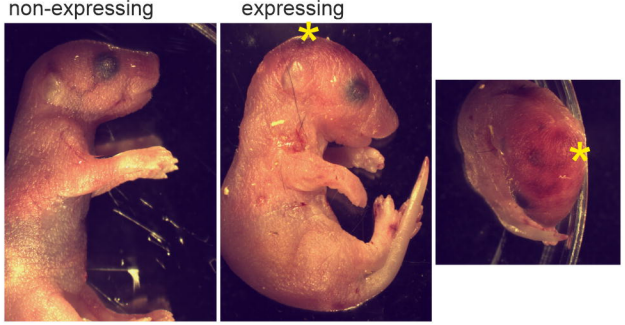

B

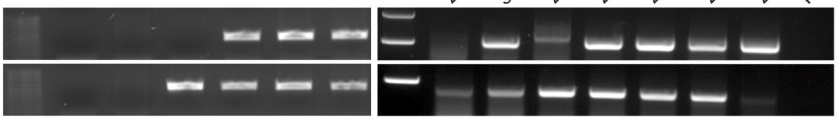

C

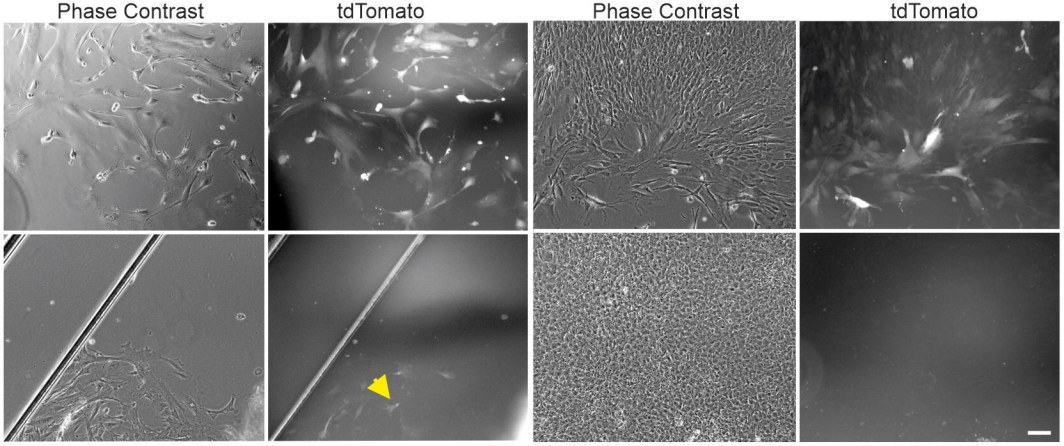

D

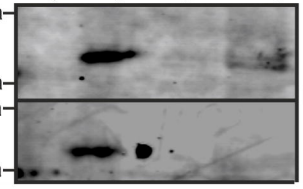

E

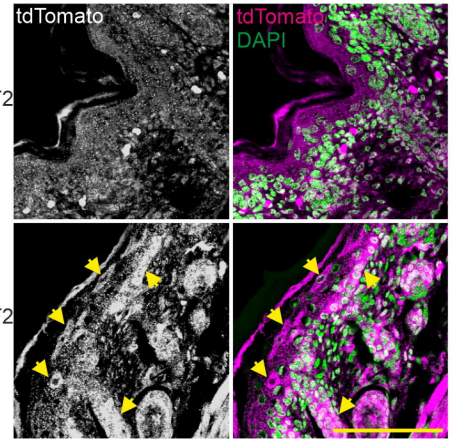

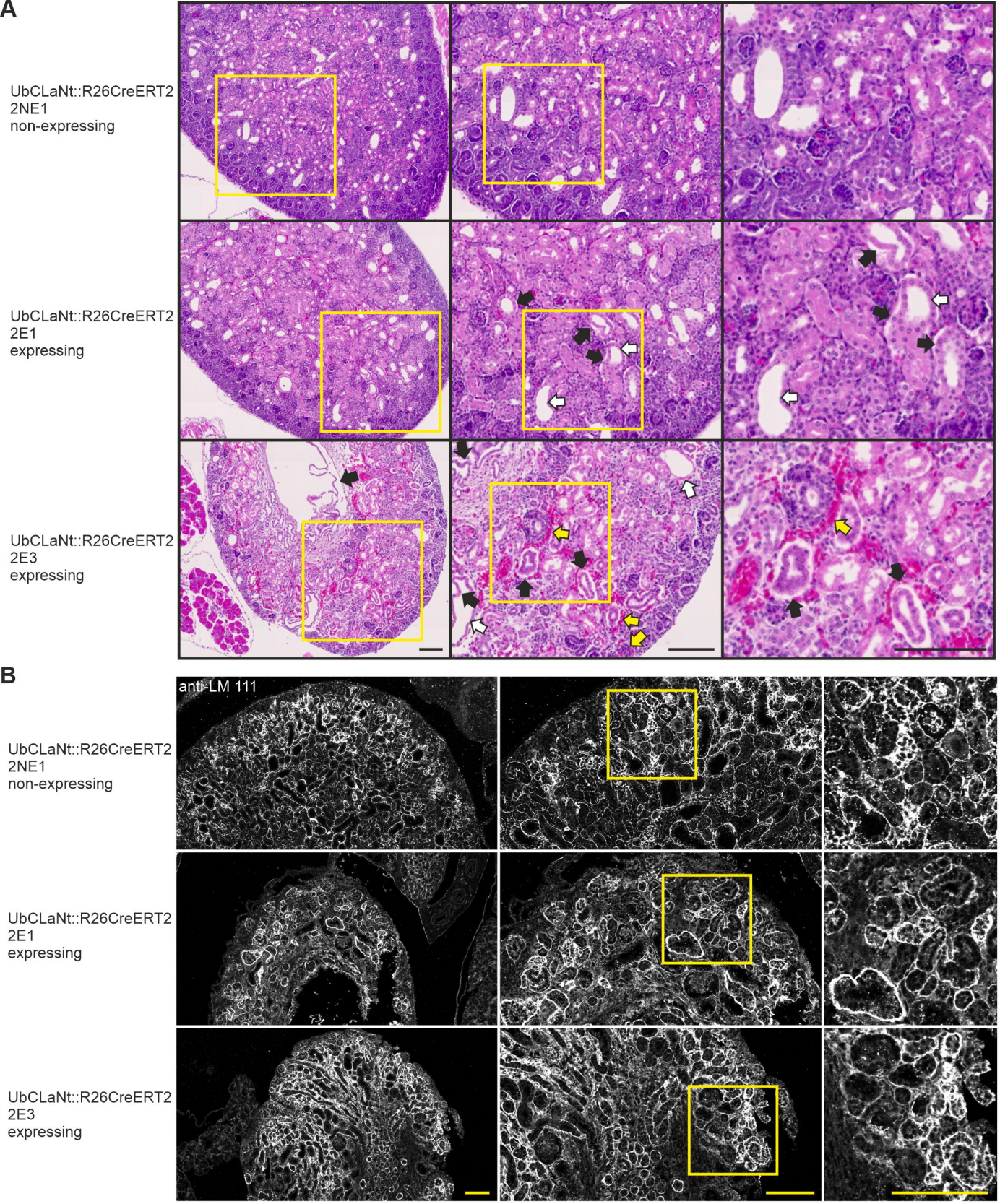
A
UbCLaNt::R26CreERT2
2NE1
non-expressing
UbCLaNt::R26CreERT2
2E1
expressing
UbCLaNt::R26CreERT2
2E3
expressing
B
anti-LM 111
UbCLaNt::R26CreERT2
2NE1
non-expressing
UbCLaNt::R26CreERT2
2E1
expressing
UbCLaNt::R26CreERT2
2E3
expressing

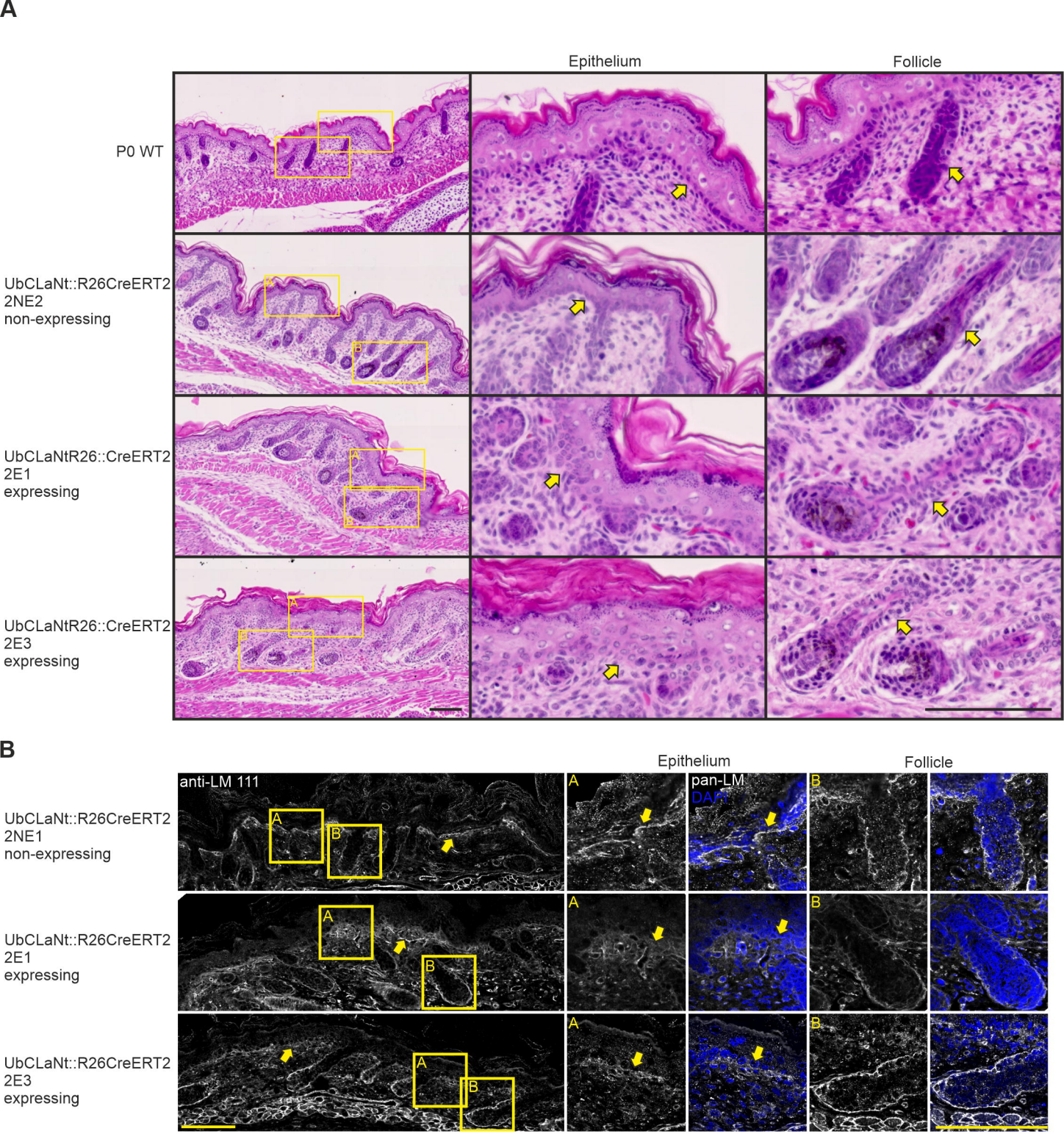
A
Epithelium
Follicle
P0 WT
UbCLaNt::R26CreERT2
2NE2
non-expressing
UbCLaNtR26::CreERT2
2E1
expressing
UbCLaNtR26::CreERT2
2E3
expressing
B
Epithelium
Follicle
anti-LM 111
pan-LM
DAPI
UbCLaNt::R26CreERT2
2NE1
non-expressing
UbCLaNt::R26CreERT2
2E1
expressing
UbCLaNt::R26CreERT2
2E3
expressing
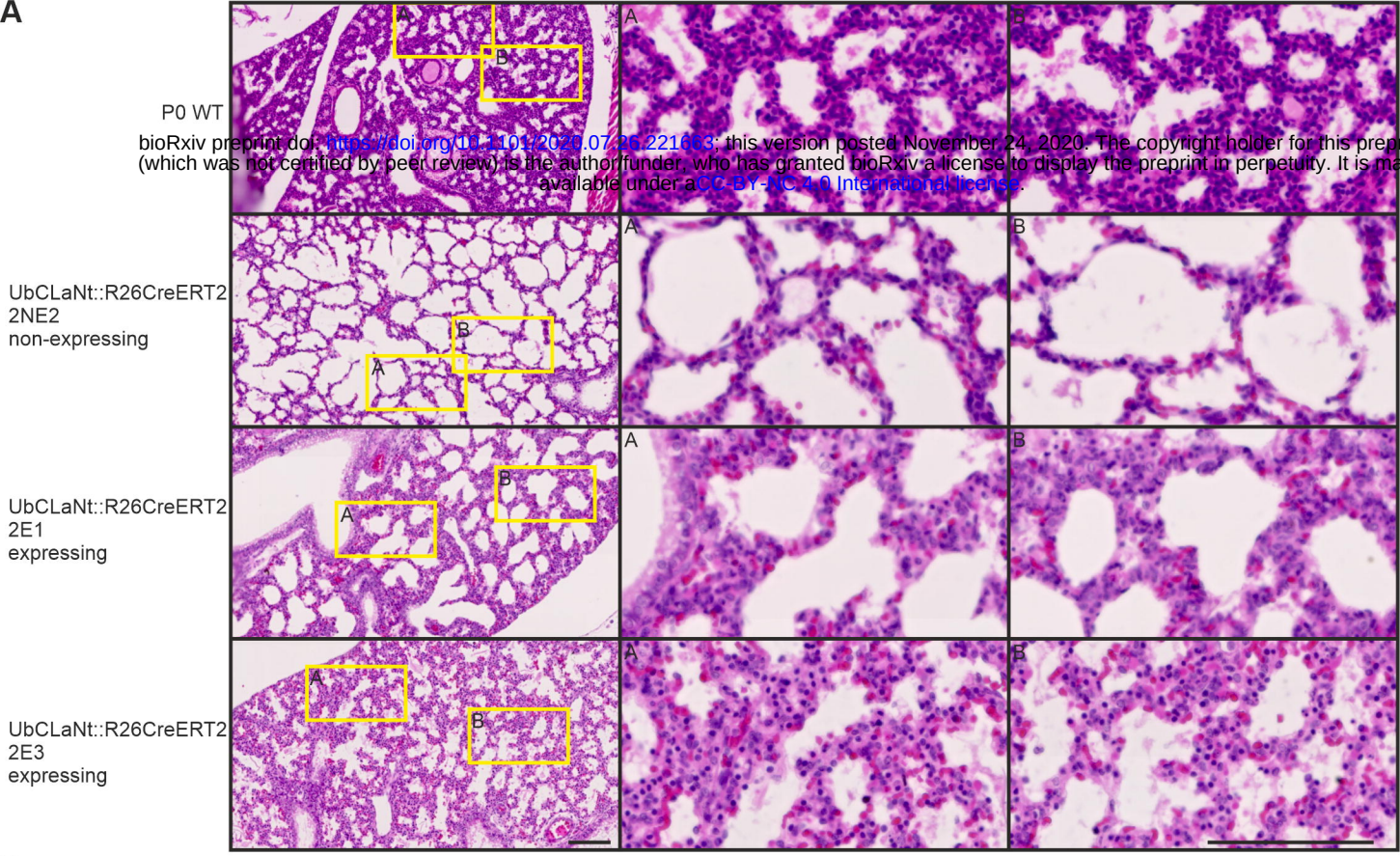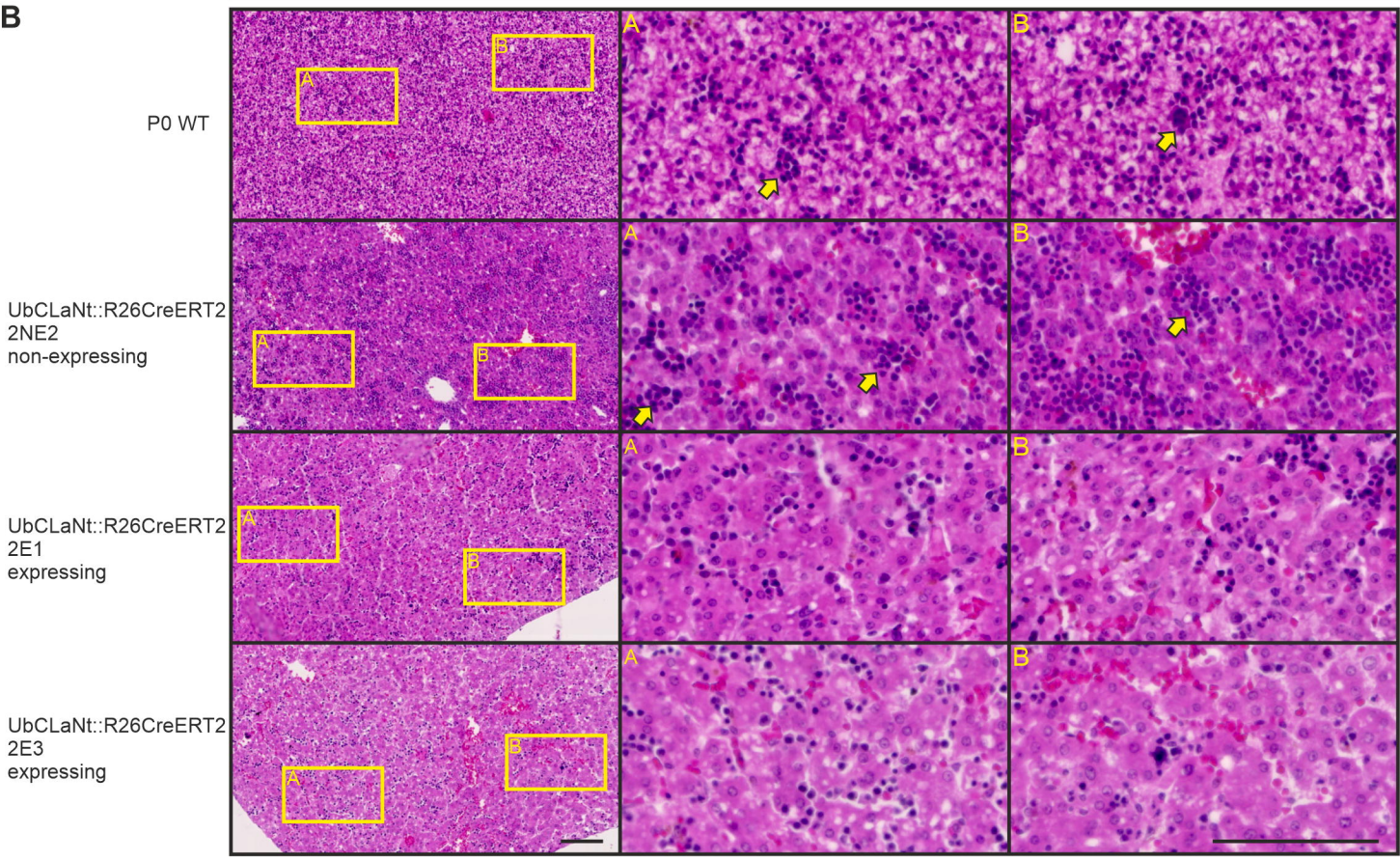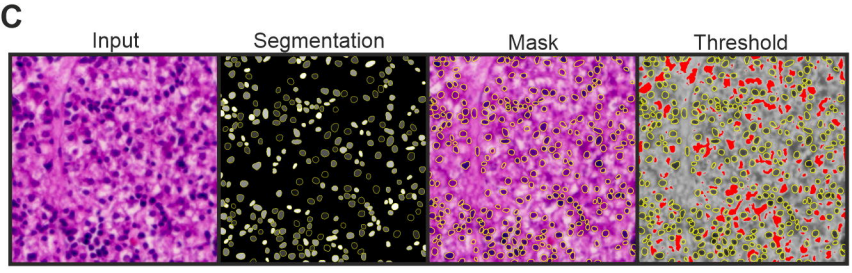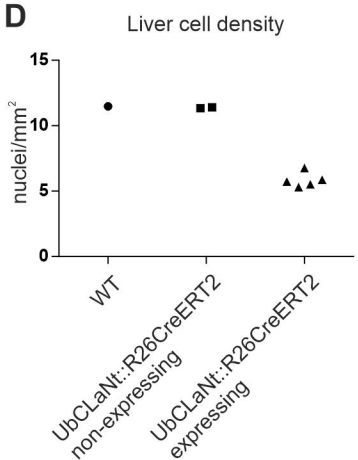
bioRxiv preprint doi: https://doi.org/10.1101/2020.07.26.221663; this version posted November 24, 2020. The copyright holder for this prepr
(which was not certified by peer review) is the author/funder, who has granted bioRxiv a license to display the preprint in perpetuity. It is ma
available under a CC-BY-NC 4.0 International license.